METABOLIC REGULATION UNDERLYING STALK SYNTHESIS IN *CAULOBACTER CRESCENTUS*

By

KEVIN DE YOUNG

A thesis submitted to the

Graduate School-Camden

Rutgers, The State University of New Jersey

In partial fulfillment of the requirements

For the degree of Master of Science

Graduate Program in Biology

Written under the direction of

Dr. Eric Klein

And approved by

_____

Dr. Eric Klein

_____

Dr. Nir Yakoby

_____

Dr. Jongmin Nam

Camden, New Jersey

May 2019

ABSTRACT OF THESIS

Metabolic Regulation Underlying Stalk Synthesis in *Caulobacter crescentus*

By

KEVIN DE YOUNG

Thesis Director:

Dr. Eric Klein

Caulobacter crescentus is a gram-negative α-proteobacterium known for its characteristic adhesive stalk and a tolerance to nutrient deprivation. Found mostly in oligotrophic (nutrient-depleted) aquatic environments, *Caulobacter* responds to changes in resource availability with dynamic metabolic and morphological alterations. We isolated a mutant strain with reduced stalk length; the mutation mapped to gene *CC3617*, a mannose 6-phosphate isomerase. During phosphate starvation, wild-type cells maintain a 1:1 ratio of mannose 6-phosphate (M6P) and fructose 6-phosphate (F6P). Our *CC3617* mutant strain, by contrast, has a relative increase in F6P. The decrease in M6P correlates with low levels of exopolysaccharide and O-antigen synthesis. Interestingly, we find that the *CC3617* mutant strain does not readily enter stationary phase; rather it continuously increases cell number and represses stationary-phase gene expression. Forced induction of stationary phase promotes stalk length recovery in the *CC3617* mutant strain. Furthermore, deletion of stationary phase genes in wild-type cells produce a reduction in stalk length.

DEDICATION

This work is dedicated to my loving girlfriend, Kerry, who has been by my side throughout all the long days and sleepless nights while I completed my research. Thank you for always motivating me to persevere during the stressful times and reminding me to “stop and smell the flowers”. I also dedicate this work to my amazing parents, Kevin and Toni, who’ve always supported me throughout good times and bad. Without your guidance this work would not be possible.

ACKNOWLEDGEMENTS

I am very thankful to my advisor, Dr. Eric Klein, for without his mentorship and friendship, this work would surely not be possible. His guidance and support in helping me to improve my experimental and analytical skills has been imperative to my growth as a scientist. Over the past four years I have witnessed his incredible work ethic, ingenious approach to problem solving and immense integrity as both a great scientist and human being. I greatly admire his knowledge, creativity, and seemingly endless capacity for patience and kindness. I am forever grateful for being allowed the opportunity to train under his guidance as my Principal Investigator and mentor. I would like to thank my committee members, Dr. Nir Yakoby and Dr. Jongmin Nam. Their advice and support have been a very helpful resource, substantially improving the quality and diligence of my work, and for that, I am grateful. I would like to thank my lab colleagues: Dr. Sudha Moorthy, Gabriele Stankeviciute and Veronica Rosselli for the productive feedback and fruitful discussions. I would like to thank Dr. Lucy Shapiro (Stanford) for providing the *Caulobacter* cosmid library and Dr. Xiaoyang Su (CINJ) for metabolomics analyses. I would also like to thank the National Science Foundation for funding my research and the Rutgers – Graduate School for selecting me for my Teaching Assistantship.

Table of Contents:

List of Figures:

Introduction:

Bacterial morphology:

Bacteria are often viewed as primitive and simplistic forms of life; However, this could not be further from the truth. Though they lack the level of organization usually attributed to "highly evolved" forms of life, bacteria are anything but "simple". Bacteria interact with their environment in dynamic ways; communicating with their surroundings and each other in a highly controlled and intricate manner. One of the most interesting and dynamic of all bacterial characteristics is an ability to dramatically modify cellular morphology in response to changing conditions. The bacterial domain exhibits a massive array of unique organisms with an enormous range of cellular sizes and morphologies, indicative of the evolutionary importance of cell shape (Young, 2006). Bacterial shape is a dynamic, responsive characteristic with many species possessing the capability to dramatically alter cell shape in response to cell-cycle progression, nutrient availability and predatory or environmental stressors. The ability to maintain and modify cellular form and composition is crucial in bacterial adaptivity and pathogenicity.

Figure.1) Cell shape variation in stalked bacteria. Top left, Caulobacter crescentus (photo Y.V. Brun, from Journal of Bacteriology 181: 1118–1125, reproduced with permission); top right, Asticaccaulis biprosthecum (photo E.M. Quardokus, from Prokaryotic Development, ASM Press, p. 297–317, reproduced with permission); bottom left, Hyphomonas neptunium (photo E.M. Quardokus, from Prokaryotic Development, ASM Press, p. 297–317, reproduced with permission); bottom right, Ancalomicrobium adetum (photo courtesy of A. Van Neerven, B. Oakley and J.T. Staley) (Wagner, et al. 2007)

The importance of bacterial morphology makes it a subject of great scientific significance and uncovering how bacteria change cell shape and composition on a genetic and physiological level are of substantial interest to scientific and medical research. Nonetheless, very little is currently understood about the function and regulation of most atypical cell forms, as it is only generally the domesticated, lab-friendly species of bacteria wherein cell shape has been thoroughly characterized. To achieve greater insight into the ways in which bacteria modulate cell shape, it is necessary to study more species of bacteria, particularly species with exotic, asymmetrical morphological characteristics to help us better understand bacteria's true breadth of morphological capabilities and the role cell morphology plays in bacterial success.

Caulobacter crescentus:

One such oddly shaped bacteria is the crescent shaped, gram-negative bacterium, *Caulobacter crescentus*. *Caulobacter* is a species of stalk-producing, α-proteobacteria found widely distributed in oligotrophic (nutrient-deprived) fresh water and marine environments (Figure 1). *Caulobacter* undergoes a unique asymmetric pattern of division, producing two unique daughter-cell forms. The dividing cell grows a characteristic tubular stalk structure that forms out of the cell envelope at one of the cell poles. The other daughter-cell form is a mobile cell that has a single flagellum accompanied by pili which provide motility. The motile cell-form will not divide until it has shed the flagella and assumed the mature stalked cell-form. Prior to stalk formation the cell pole secretes an extremely adhesive polysaccharide that anchors the cell to surfaces where the cell remains constitutively fixed as it readily divides, giving rise to motile daughter cells (Figure 2). This adhesive is retained at the tip of the stalk (Hughes, et al. 2012).

Figure.2) Schematic diagram of the C. crescentus cell cycle. The three different cell types of C. crescentus, the stalked cell, the swarmer cell, and the pre-divisional cell are depicted with polar appendices underlined. The clockwise orientation of the cell cycle is indicated by arrows. The developmental and cell cycle events described in the text are highlighted at the time when they take place during the life cycle. The Caulobacter cell cycle is divided into three distinct phases: The G1-phase includes the motile stage and the swarmer-to-stalked cell transition; the S-phase decides the period of active chromosome replication; the G2-phase outlines cytokinesis and cell division stages. The length of the S-phase is identical for both the newly differentiated (unexperienced) stalked cell and the (experienced) stalked cell emerging from cell division (Jenal, 2000)

In a morphological sense, *Caulobacter* stalks are appendages that are unique in many regards. The stalk itself is an extrusion of the cell body through a thin filamentous polar outgrowth (Schlimpert, et al. 2012). As the stalk elongates, new stalk material is synthesized at the base which initially forms following a series of signaling events carried out by polar marker proteins that choreograph the cell-cycle processes leading to the loss of the flagella, and the subsequent formation of a stalk at the same cell pole (Hughes, et al. 2012).

Stalk composition:

Caulobacter stalks are a polar extrusion of the entire cell envelope, being synthesized at a single cell pole via a cytoskeletal complex that forms upon flagellar shedding. This includes a polysaccharide-derived capsule, proteinaceous crystalline S-layer, outer membrane with an outer leaflet composed primarily of lipopolysaccharide and an inner leaflet composed of phospholipid species, periplasmic cell wall and an inner membrane composed primarily of phospholipids. Additionally, like most cellular membranes, the inner and outer membranes are largely composed of proteins (Jenal, 2000; Schlimpert, et al. 2012). The end of the stalk possesses an adhesive holdfast composed of polysaccharides that allow for the permanent anchoring of the cell to a surface (Figure 3). Although Caulobacter stalks are generally identical to the cell envelope of the cell body, several unique compositional characteristics have been identified. Uniquely, as the stalk elongates, it is compartmentalized periodically with proteinaceous diffusion barrier complexes (stpABCD) that divide the stalk's cytoplasmic and periplasmic regions into isolated chambers (Figure 4). Once sealed, any proteins or large molecules are believed to be irreversibly sealed within the stalk compartments (Klein, et al. 2013).

Figure.3) Caulobacter stalks are polar extrusions of the entire cellular envelope; predominantly identical in composition to the cell body. The stalk interior is regularly compartmentalized by proteinaceous diffusion barriers as it elongates. (Lohmiller, et al. 2008)

*Figure.4) (A) StpAB-deficient cells consistently lack crossbands. Cells with and without stpAB (SW51, n = 8) were grown in PYE and imaged by ECT. The images show a longitudinal section of the stalk. Asterisks denote crossbands. Arrowheads point at unidentified structures spanning the stalk core. Scale bars: 100 nm. (B and C) The distribution of StpB-mCherry foci reflects the distribution of crossbands in stalks. Cells of strains CB15N (WT) and SS160 (stpB-mcherry) were grown in M2G−P and imaged either by electron (EM) or fluorescence (FM) microscopy, respectively. Electron micrographs were acquired of negatively stained wild-type cells. From the respective images, the number of crossbands (n = 68 cells) and StpB-mCherry foci per μm stalk (n = 316 cells) was quantified (*p > 0.2, t-test; error bars = SEM). Asterisks denote crossbands. Scale bars: 500 nm (EM) and 3 μm (FM). (D) StpB spatially overlaps with crossbands. Strain SW30 (Pxyl::Pxyl-stpB-mcherry) was grown in M2G−P with 0.3% xylose. Cells were fixed on EM grids and imaged first by low-magnification phase contrast/fluorescence microscopy (inset; arrowheads indicate StpB-mCherry foci) and then by ECT. Shown is an ECT slice of a stalk with arrows pointing to crossband structures (left panel) and the respective correlated image showing the ECT slice overlayed with a fluorescence micrograph of the same region (right panel). Scale*

bar: 100 nm. (E) FRAP analysis reveals that crossbands are static protein complexes. Cells of strain SS160 (stpB-mcherry) were cultured in M2G−P and imaged by fluorescence microscopy to identify StpB-mCherry localization. A laser pulse was applied to selected regions (yellow circles), and StpB-mCherry signals were bleached. Cells were imaged immediately and 10 min after the laser pulse. Scale bar: 3 μm. (Schlimpert, et al. 2012)

Additionally, stalk-specific modifications to cell wall synthesis have been recently identified by the Klein lab. The cell wall is an encapsulating matrix spanning the entirety of the cell envelope, existing in between the inner and outer membranes, supplying the cell with structural rigidity. It is composed of peptidoglycan; a heterogeneous polymer composed of alternating repeats of N-acetyl-glucosamine and N-acetyl-muramic acid connected by peptide chains. The peptide chains can be alternatively connected between different amino acids in two variations; referred to as D-D and L-D crosslinks. Peptidoglycan in *Caulobacter* cell bodies have been found to consist almost exclusively of D-D crosslinks while stalk peptidoglycan contains an increased percentage of L-D crosslinks (Stankeviciute, et al. 2019).

Stalk response to phosphate starvation:

Caulobacter stalks initially form in accordance with cell cycle cues; forming a stalk after a short-lived motile period and subsequently replacing the shed flagella and pili with the newly formed stalk. Initial stalk synthesis results in a small stalk, rarely exceeding the length of the cell body; however, *Caulobacter* undergo a unique response to phosphate-depleted conditions wherein the polar stalk begins to rapidly and extensively elongate, growing to many times the length of the cell body over the course of several days (Gonin, et al. 2000). These unique characteristics make *Caulobacter* stalk synthesis and regulation an extremely interesting topic of research concerning cell shape, as it is a dramatic and

precisely controlled modification of bacterial morphology that occurs under the control of cell-cycle and conditionally in response to environmental status. The underlying purpose of *Caulobacter* stalks, and the dramatic increase in stalk length observed upon phosphate starvation, is still somewhat unclear, though it is likely attributed to functions put forth in several hypotheses (Figure 5). One theory holds that stalks allow *Caulobacter* to efficiently increase their functional cell length without expending material on excess surface area and increased cytoplasmic volume. It has been shown that nutrient flux scales with cell length more so than total cell surface area, so it is possible that *Caulobacter* acquire more phosphate through stalk elongation as opposed to elongating the cell body alone (Klein, et al. 2013).

Figure. 5) Models for the physiological role of stalk elongation. (A) The red pathway describes the previously held model of phosphate uptake, in which PstS shuttles phosphate from the stalk to the cell body, where it is imported by the PstCAB transporter.6 Our discovery of a diffusion barrier which blocks PstS shuttling contradicts this model.5 An alternative model, shown as the green pathway, assumes that previously undetected PstCAB complexes do exist in the stalk, allowing the uptake of phosphate into the cytoplasmic core of the stalk and its subsequent diffusion to the cell body. (B) Using kinetic and diffusion parameters, the distance that PstS-phosphate complexes can diffuse before phosphate release is approximately 0.7 µm. This distance is far shorter than the stalk length under phosphate-limiting conditions. (C) Localization of PstA-GFP in the stalk. Strain YB4062 (CB15N pMR10-Ppst-pstCA-gfp) was grown for 36 h in HIGG medium containing 30 µM phosphate. PstA-GFP was visualized by fluorescence microscopy. Arrowheads indicate stalks containing the fusion protein. Scale bar: 2 µm. (D) Subcellular localization of Heat Shock Protein 20 (HSP20, IbpA homolog) in wild-type and ΔstpAB cells grown in high-phosphate (PYE) and in low-phosphate (M2G−P) medium. To test for the segregation of damaged proteins into the stalk, cells of strains SS419 (CB15N

Pxyl::Pxyl-ibpA-venus) and SS420 (CB15N ΔstpAB Pxyl::Pxyl-ibpA-venus) were first grown in M2G−P for 12 h. Production of IbpA-Venus was induced by adding 0.3% xylose for 1 h prior to a heat shock. Cells were shifted to 40°C for 1 h, followed by a growth period of 8 h at 28°C. Untreated cells were cultured at 28°C for 9 h. Images show overlays of DIC and false-colored fluorescence images. Scale bar: 3 µm. (E) Stalk elongation may function to elevate single cells away from surfaces. As the cell distances itself from the surface, fluid velocity (blue gradient) and nutrient flux (blue arrows) increase. Thus, stalk elongation may ensure greater nutrient availability. (F) Caulobacter cells may co-colonize surfaces with other organisms. By distancing themselves from the surface, they may have greater access to nutrients relative to nearby surface-associated species, thereby increasing their competitiveness (Klein, et al. 2013).

An alternative hypothesis for the adaptive advantage of *Caulobacter* stalk elongation under phosphate limitation proposes that stalk lengthening changes the spatial position of the cells by rising above the anchor point, allowing the cell body to extend out into a more nutrient rich zone (Klein et al. 2013). This theory is based on the understanding that nutrients in a flowing fluid system exhibit increasingly less convective dispersal closer to the bordering surface, eventually reaching zero velocity at the surface boundary. This phenomenon is referred to as the "no-slip boundary condition" in the study of fluid dynamics (Zhu et al. 2002). This means that *Caulobacter* anchored close to a surface will only primarily receive nutrients through the far less efficient means of passive diffusion. An increase in distance from the surface by 10µm would result in a 10% increase in nutrient interaction (Klein et al. 2013). Furthermore, fellow *Caulobacter* and other biofilm forming bacteria may crowd the surrounding surface in a natural environment, interfering with the acquisition of nutrients and the dispersal of new cells. By lengthening the stalk, *Caulobacter* can rise above the surface where it can orient the cell body, capable of intaking phosphate, into a more nutrient-rich position along the convective fluid gradient, up and away from competing neighbors (Klein et al. 2013). Despite these hypotheses of why *Caulobacter* stalks elongate in phosphate poor conditions, the actual mechanisms by which

Caulobacter cells regulate their response to phosphate starvation are incompletely understood.

Genetic regulation of stalk formation:

As previously discussed, phosphate starvation is the prominent causative triggering event of stalk elongation in *Caulobacter*. Phosphate enters the outer membrane initially through both passive and active diffusion through a host of selectively-permeable outer membrane proteins (OMP's), including BAM complex β-barrel porins, several homologs of the monomeric porin protein, OmpA, and TonB-dependent receptors (Ryan, et al. 2010). After passing through the outer membrane, phosphate binds with the periplasmic protein, PstS, where it is shuttled to the inner membrane, ultimately being transported by the inner membrane PstCAB complex. PstCAB associates with the membrane-associated proteins, PhoU and PhoR. In excess phosphate, PstCAB represses the auto-phosphorylation of the histidine kinase, PhoR. Upon phosphate starvation, the PstCAB complex disengages with PhoR through interactions with PhoU, allowing it to auto-phosphorylate and continue on to phosphorylate the cytoplasmic transcription factor, PhoB. Phosphorylated PhoB binds to a series of promoters, known as the "Pho box," promoting the upregulation of *pstCAB* and associated genes, in addition to an increase in stalk synthesis (Figure 6) (Gonin et al. 2000).

Figure. 6) Model of the Pho regulon and organization of pst and pho genes of Caulobacter. (A) The Caulobacter life cycle and effect of phosphate starvation. The life cycle of swarmer cells is depicted. The newborn swarmer cell spends an obligatory period of its life cycle as a chemotactically competent polarly flagellated cell unable to initiate DNA replication. Stalk synthesis is initiated at the pole that previously contained the flagellum coincidently with the initiation of DNA replication during the swarmer-to-stalked cell differentiation. The new stalked cell elongates, initiates cell division, and synthesizes a flagellum at the pole opposite the stalk, giving rise to an asymmetric predivisional cell. Cell division yields a stalked cell that can immediately initiate a new cell cycle and a swarmer cell. Phosphate starvation yields elongated cells with long stalks. (B) Model of the Pho regulon. This model is adapted from work with E. coli. The PstSCAB proteins form the high-affinity phosphate transport system. When phosphate is in excess, the Pst complex represses the autophosphorylation of the histidine kinase PhoR. PhoU is required to inhibit the expression of the Pho regulon,but is not required for phosphate transport by the Pst system. Deletion of phoU has deleterious effects on growth, and these effects are dependent on phoB. When cells are starved for phosphate, the Pst complex releases PhoR, which autophosphorylates and transfers the phosphate residue to PhoB. PhoB∼P binds to the Pho box sequences of promoters (−10 and bent arrow) and activates the transcription of most genes of the Pho regulon. In a few cases, binding of PhoB-∼P represses transcription. We hypothesize that PhoB∼P activates the transcription of a gene or genes whose expression results in an increase in stalk synthesis. (C) Organization of the pst-pho gene cluster. Genes are represented by arrows, and the sites of transposon insertion in the different mutants are represented by "lollipop" structures. The thick line labeled PCR under the region between pstC and pstA indicates the PCR product that was obtained with oligonucleotides from the end of the phoR-pstC sequence contig and the beginning of the pstA-pstB-phoU-phoB sequence contig. The pstS gene is shown below the pst-pho region because it maps to an unlinked locus. (Gonin et al, 1999)

Interruption of the phosphate uptake and recognition systems has been observed to cause stalk perturbations; with stalk deficiency observed in Δ*bamE* and *phoB*Ω12 mutants and stalk elongation occurring in phosphate-rich media upon perturbation of PstS (Gonin, et al. 1999; Ryan, et al. 2010). In addition to phosphate regulated genes, the majority of what has been found about stalk synthesis-specific mechanisms focus predominantly around cell wall (peptidoglycan) synthesis machinery. It is known that MreB, the bacterial homolog of actin, is the major component of general bacterial cell wall synthesis; however, it has been observed that MreB concentrates at the cell pole during *Caulobacter* stalk synthesis. MreB perturbations have been found to result in stalk deficiencies in addition to cell body malformation (Wagner. et al. 2005). In addition to MreB, several other proteins

have been found to play a supportive or essential role in stalk-related peptidoglycan synthesis (Figure 7). Penicillin-binding proteins (PBP), are the enzymes responsible for PG production via transpeptidation and transglycosylation (Yakhnina 2013). PBP's have been found to play a direct role in the proper function of stalk biogenesis and elongation. PbpC is one of five PBP's known in *Caulobacter* and has been shown to have the greatest role in stalk synthesis. Disruption of PbpC leads to a 25% reduction in stalk length. Deletion of other PBP's, even in combination, shows a negligible effect on stalk length, indicating a high level of redundancy among this class of proteins in *Caulobacter* (Yakhnina 2013). PbpC has been shown to be recruited to the cell pole via a transmembrane polar protein complex formed by BacA and BacB, two classes of bactofilin proteins. Deletion of these bactofilins, especially BacA, results in a 45% reduction in stalk length. It is hypothesized that the stalk effect is caused by an inability to properly recruit PbpC to the stalk-forming pole (Kuhn 2010). Additionally, the genes RodA and RodZ, which establish interactions with the MreB transmembrane protein complex, exhibits cell body abnormalities and stalk synthesis defects upon perturbation (Wagner, et al. 2005).

Figure. 7) Model depicting MreC interactions with cytoplasmic and outer membrane proteins. Internal MreB helices (green) lying underneath the cytoplasmic membrane are proposed to be the master organizer of the spatial distribution of proteins that lie outside the cytoplasm. These include PBP complexes (multicolored; inner membrane) that are anchored in the cytoplasmic membrane but have the bulk of their polypeptide in the periplasm, the periplasmic MreC protein (red), and a subset of outer membrane proteins (multicolored; outer membrane). The experiments presented here demonstrate that MreC interacts with both PBPs and several outer membrane proteins. We propose that MreC plays a critical role in helping establish or maintain these proteins in their patterns of localization, perhaps linking, through some intermediary membrane protein, the PBPs and outer membrane proteins to the internal MreB cytoskeleton (Divakaruni, et al. 2005)

In addition to cell wall machinery, various signaling events driving stalk synthesis are known to occur involving major cell-cycle regulators and polar marker-determinant proteins, such as: CtrA, CC2105, DivJ, DivK, PleC and SpmX which result in either multiple or ectopic stalk formation upon their perturbation (Perez, et al. 2017). There is still much about the regulatory and biosynthetic mechanisms of *Caulobacter* stalks that are

not understood. Many of these perturbations result in only modest reductions of stalk functions, showing a redundancy and resiliency of the stalk-forming system, likely indicating the presence of a much more complex system than is currently understood. Most known stalk-related genes are primarily grouped into either phosphate uptake and recognition genes, peptidoglycan synthetic machinery or signaling proteins, and the complete connection between phosphate starvation, cell-cycle cues and polar peptidoglycan machinery recruitment are incompletely understood. My research has uncovered a novel relationship between phosphate starvation-induced stalk elongation, stationary phase induction and the global metabolic flux of sugar phosphates.

Experimental methods:

Bacterial growth conditions:

Caulobacter strains were grown at 30°C in peptone-yeast extract (PYE) medium for routine culturing and storage. To control phosphate levels, *Caulobacter* was grown in Hutner base-imidazole-glucose-glutamate media (HIGG) with variable amounts of phosphate (1μM-1mM). HIGG carbon sources were modified for certain experiments, replacing glucose with mannose, fructose and deuterated glucose (D2-Glucose). *E. coli* strains were grown at 37°C in LB medium. When necessary, antibiotics were added. Gene expression was induced in *Caulobacter* with either 0.003-0.3% (w/v) xylose or 0.5mM vanillate. *E. coli* gene expression was induced with 0.5mM IPTG and grown at 22℃. For selective recombination, Caulobacter cells were grown on PYE plates with 0.3% sucrose.

Cosmid complementation:

A genomic cosmid library was obtained from Lucy Shapiro (Stanford University) which consists of 192 genomic fragments in *E. coli* hosts accounting for the nearly complete genome coverage of wild-type *Caulobacter*. The cosmid library was used to conjugate large segments (approximately 30-50kb) of the wild type *Caulobacter* genome into the stalk-deficient mutant in attempt to recover normal stalk functionality via genetic complementation of identified mutations in the sequenced mutant genome. Successful conjugations were identified through antibiotic selection via tetracycline resistance obtained from the cosmid vector. The cosmid-containing *E. coli* were grown overnight in liquid LB with tetracycline at 37℃.

Stalk mutants were grown overnight in PYE (peptone yeast extract) at 30℃. Once grown, 100μL of cosmid *E. coli* culture is mixed with 1mL of the stalk mutant culture (1:10) and centrifuged at 8000 RPM for 2 minutes. The supernatant is discarded and the bacterial pellet is remixed into 10μL of PYE which is then plated on a prewarmed PYE plate. The conjugants are incubated at 30℃ overnight and then streaked out on a PYE Tet + Nalidixic acid plate and allowed to incubate at 30℃ for two to three days until colonies become visible (*Caulobacter* possess a natural resistance to nalidixic acid while *E. coli* do not). The conjugant colonies are isolated and grown in PYE tet liquid media from which freeze downs are made.

Protein purification:

Multiple proteins were purified for study including: CC3617, RffE and RffD. All proteins were cloned into the high-copy inducible plasmid pET28a, Kan^R containing a poly-His tag for protein purification, and subsequently transformed into *E coli* strain BL21. Transformed BL21 strains were grown overnight in LB Kan at 37℃ and back diluted 1:100 into LB Kan + 0.5mM IPTG to induce protein expression. Cultures were grown at 22℃ overnight in incubator. Cells were then pelleted and frozen overnight at -20℃. Protein was extracted via column purification using a cobalt-based extraction resin. Protein was extracted from the resin using a series of increasingly concentrated imidazole washes which compete for cobalt binding with the recombinant proteins His-tag. Proteins were aliquoted into 100μL volumes and stored at -20℃.

Enzyme kinetics assay:

CC3617 activity was determined using a modified protocol of the Fructose Assay Kit (SIGMA product code: FA-20). Modification included substitution of fructose with

mannose as a substrate then adding CC3617 to the mixture to convert M6P into F6P where it completed the standard enzyme assay.

Suppressor mutant generation and isolation:

SDM2 was streaked on PYE plate and incubated for two days at 30℃. A single colony was chosen and grown up in 2mL of HIGG (Hutner Imidazole Glucose Glutamate) 1mM phosphate overnight at 30℃. 1mL was pelleted and frozen at -20℃ for sequencing. The remaining culture was washed twice in zero phosphate HIGG to remove phosphate and added to 100mL culture of HIGG 1μM phosphate and allowed to grow for 2 days at 30℃. After two days, the culture is centrifuged at 10,000g for 10 minutes. The supernatant was removed and spun in an ultracentrifuge at 28,000g for 30 minutes. Pelleted cells were then resuspended in 750μL of HIGG 1μM phosphate and put back into 20mL of HIGG 1μM phosphate. Subsequent spins and back dilution continued in 20mL volumes from this point on for two weeks. After two weeks, an aliquot of the culture was streaked on PYE naladixic acid plates (to remove any contamination) and allowed to grow for 3 days at 30℃. Colonies were subsequently picked and grown in HIGG 1μM phosphate to induce stalk growth for two days. Cells were imaged for stalk recovery. Identified suppressor mutants were frozen down at -80℃ and samples were taken for sequencing.

Growth curves:

Growth curves were conducted using two methods depending on length of growth analysis. Growth curves of 24 hours or less were done in 96 well plates and measured using the CLARIOstar microplate reader. Samples were done in multiples, consisting of 150μL culture samples and 100μL mineral oil atop each sample to minimize evaporation. Wells were measured for absorbance at 660nm every 20 minutes (73 cycles) and gently shaken.

For growth curves longer than 24 hours, cells were grown in test tubes and measured periodically via a Bio Rad SmartSpec 3000 spectrophotometer using cuvettes at an absorbance of 660nm after being blank corrected for media absorbance. All growth curves were conducted at 30°C

Stress test:

NA1000 and SDM were grown in PYE overnight. Stock solutions of 75x MIC concentration of toxic agents was prepared: Tetracycline (33.75μg/mL), Bacitracin (50 μg/mL), Vancomycin (3 mg/mL), SDS (0.34% w/v) and $ZnSO_4$ (22.5mM) and subsequently prepared into 1.5-fold serial dilution (7 total). Cells were back diluted to an OD_{660} of 0.01 in a 96-well format and serial dilutions of each toxin was added to cultures including a negative control (8 wells total). Growth curves were conducted per the protocol listed above for a 16-hour cycle to assess cell envelope integrity.

Peptidoglycan analysis:

For whole *Caulobacter* cells, we started with 500-mL cultures grown in either high-phosphate (1 mM) or low-phosphate (1 μM) HIGG growth media. To mechanically detach stalks from cell bodies, cells from 3 L cultures were sheared in a standard kitchen blender for 1 min at maximum speed. For mechanically sheared cells and the stalk-shedding YB2811 strain, cell bodies were purified by low-speed centrifugation (10 min at 8000 × g, 4°C); excess cell bodies were removed via 2–3 spins for 10 min at 10,000 × g. The removal of cell bodies was examined by microscopy. Subsequently, stalks were harvested from the washed supernatant (1 h centrifugation at 47,056 × g). Peptidoglycan muropeptides were purified from *Caulobacter* as previously described (Desmarais et al., 2014) and separated on a reversed-phase C18 column (Thermo Scientific; 250 × 4.6-mm column, 3-μm particle

size) held at 55°C. The LC solvent system consisted of 50 mM sodium phosphate [pH 4.35] with 0.4% sodium azide (solvent A) and 75 mM sodium phosphate, pH 4.95 + 15% (v/v) methanol (solvent B). The solvent flow rate was 0.5 mL min–1 and a linear gradient to 100% sol-vent B was performed over 135 min. Muropeptide elution was monitored at 205 nm and sample fractions were collected at time points as indicated.

Lipopolysaccharide analysis:

NA1000 and SDM2 cells were grown in 5mL HIGG 1μM phosphate until OD_{660} of 0.5 was achieved. Cells spun down at 10,000g for 10 minutes and washed with 10 mM HEPES, pH 7.2. Cells spun down at 10,000g for 10 minutes, HEPES removed and cells were subsequently resuspended in 250μL 10 mM Tris-1mM EDTA, and frozen at -20℃. Samples were thawed, combined with 1 μl DNase (0.5 mg/ml), 20 μl lysozyme (10 mg/ml), and 3 μl 1 M MgCl2, and incubated at room temperature for 15 min. The above mixture (38.75 μl) was then combined with 10 μl of 4× SDS dye, incubated at 100°C for 10 min, and cooled to room temperature. Proteinase K (1.25 μl of a 20-mg/ml stock solution) was added, and the sample was incubated at 60°C for 1 h as previously described (Cabeen, et al. 2010). Samples were analyzed on 12% acrylamide gels using the Pro-Q Emerald 300 Lipopolysaccharide Gel Stain Kit (P20495)

EPS assay:

NA1000, CB15 and SDM2 cells were streaked onto HIGG zero phosphate plates supplemented with 3% (w/v) sucrose and allowed to grow until biofilms became visible. Plate was imaged using a UVP MultiDoc-it Imaging System for mucoidal appearance.

Microscopy:

All images were taken with a Nikon Eclipse Ti microscope at 150x magnification with oil immersion. Images were analyzed on Nikon software. Samples were imaged on 1% agarose pads prepared on glass slides.

Stalk measurements:

All stalk lengths were measures using Image J image analysis software and quantified on Origin PRO data analysis software.

Metabolomics and metabolite extraction:

NA1000 and SDM2 were grown in triplicate in 5mL cultures in HIGG 1mM phosphate overnight in 30℃. Cells were back diluted into 10mL cultures of HIGG 1mM phosphate and allowed to grow to 0.3 OD_{660}. Once achieved, 5mL samples were vacuum filtered onto 0.2μm nylon filters and subsequently submerged upside down in 1.2mL of an ice cold solution of acetonitrile:methanol:H_20 [2:2:1] in a small petri plate and placed at -20℃ for 15 minutes. Solvent was used to wash filters then transferred to a 2mL Eppendorf tube containing 50mg of 0.1mm glass beads. Tubes were shaken in a Qiagen Tissuelyser II for 5 minutes at 30Hz. The solvent was immediately neutralized using 100μL of 1.9M NH_4HCO_3. Tubes were centrifuged to remove glass beads and the supernatant was placed in new 1.5mL Eppendorf tubes and stored at -80℃ prior to metabolomics analysis at the Cancer Institute of New Jersey. The remaining 5mL of culture was centrifuged at 10,000g for 10 minutes and washed twice in HIGG zero phosphate to remove phosphate. Once washed, cells were resuspended in 5mL of HIGG 1μM phosphate and allowed to grow for 6 hours at 30℃. Phosphate starved cells were subsequently processed in the same method

described above after 6-hour period. This protocol was repeated with deuterated glucose to allow for the detection of F6P and M6P separately.

qRT-PCR:

For stationary phase qRT-PCR, cells were grown in triplicate for 48 hours in HIGG 30μM phosphate. Cells were then back diluted into 50mL of HIGG 30μM phosphate to an OD_{660} of 0.03 and allowed to grow for 48 hours. RNA samples were collected at the 6, 24, and 48-hour mark and analyzed for expression levels of stationary phase genes: *katG, spdR, cspD*. For phosphate detection qRT-PCR, cells were grown in triplicate in 10mL of HIGG 1mM phosphate overnight at 30°C. 5mL of cells were collected and RNA extracted for high phosphate group. Remaining cells were pelleted and washed three times in ice cold HIGG zero phosphate. Cells were then resuspended in HIGG zero phosphate and allowed to grow for 5 hours as previously described (Gonin, et al. 1999). Cells were collected via centrifugation (10 min, 3800 × g, 4°C) and resuspended in Bacterial RNA Protect (Qiagen) in accordance with the manufacturer's protocol. RNA was purified using the RNeasy Mini Kit (Qiagen) and contaminating DNA was removed via DNase treatment. Purified RNA (5 ng μL^{-1}) was reverse-transcribed using the ABI High Capacity cDNA Reverse Transcription kit. Control samples did not contain reverse transcriptase to assess the level of DNA contamination. cDNA was amplified using Power SYBR Green Master Mix (Thermo Scientific) and analyzed on a Quantstudio 6 instrument (Thermo Scientific).

Strain construction**:**

Creation of the various *Caulobacter* chromosomal point-mutation strains was done by double-homologous recombination using both positive and negative selection. The suicide plasmid pNPTS138 has both a kanamycin resistance cassette as well as

the *sacB* gene which is toxic in the presence of sucrose. Genomic fragments (1000 bp) centered on the chromosomal region of interest were ligated into the pNPTS138 vector. The plasmid was transformed into *Caulobacter* and recombinants were selected on kanamycin plates. Individual colonies were grown overnight in PYE (without antibiotic) and streaked out onto PYE-3% sucrose plates to recover colonies that performed the second recombination. Colonies were screened for the gene deletion by PCR and streaked out onto plain PYE and PYE-kanamycin plates to confirm the loss of the plasmid backbone.

Strain KD145 (NA1000*::CC3617*$^{A23T/G339N}$(SDM2)) was cloned by PCR amplifying the *CC3617* locus from SDM1 genomic DNA with primers EK758/761. This fragment was ligated into the HindIII/EcoRI site of pNPTS138. The assembled plasmid (pKD186) was electroporated into NA1000 followed by selection on PYE-kanamycin plates. An individual colony was grown overnight in PYE and streaked onto PYE-3% sucrose plates. Colonies were screened visually for a stalk elongation defect and the SNPs were confirmed by DNA sequencing.

Strain KD175 (NA1000*::CC3617*^{A23T}) was cloned by PCR amplifying the *CC3617* locus from NA1000 genomic DNA with primers EK758/761. This fragment was ligated into the HindIII/EcoRI site of pNPTS138. The A23T SNP was introduced by inverse-PCR using primers EK742/743. The assembled plasmid (pKD185) was electroporated into NA1000 followed by selection on PYE-kanamycin plates. An individual colony was grown overnight in PYE and streaked onto PYE-3% sucrose plates. Colonies were screened by amplifying genomic DNA with primers EKS188/740 and digesting with PpuMI (wild-type: 509 bp, A23T: 348 and 161 bp).

Strain KD174 (NA1000*::CC3617*^{G339N}) was cloned by PCR amplifying the *CC3617* locus from NA1000 genomic DNA with primers EK758/761. This fragment was ligated into the HindIII/EcoRI site of pNPTS138. The G339N SNP was introduced by inverse-PCR using primers EK887/888. The assembled plasmid (pKD184) was electroporated into NA1000 followed by selection on PYE-kanamycin plates. An individual colony was grown overnight in PYE and streaked onto PYE-3% sucrose plates. Colonies were screened by amplifying genomic DNA with primers EKS191/Q42R and digesting with HpyCH4III (wild-type: 436 and 34 bp, G339N: 227, 209, and 34 bp).

Strains KD160 (*CC3617::CC3617-mCherry*), KD161 (*CC3617***::CC3617***-mCherry*), and KD162 (-13ΔC *CC3617***::CC3617***-mCherry*) were cloned by Gibson assembly. The 5'-arm of *CC3617* was PCR amplified from NA1000 or SDM2 genomic DNA with primers EK985/986; mCherry was amplified from pXCHYC-5 using primers EK987/988; the 3'-arm of *CC3617* was amplified from genomic DNA using primers EK989/990. Plasmid pNPTS138 was amplified with primers EK897/898. The assembled plasmids (pKD158 and pKD159) were electroporated into NA1000, SDM2, or Suppressor mutant followed by selection on PYE-kanamycin plates. An individual colony was grown overnight in PYE and streaked onto PYE-3% sucrose plates. Colonies were screened by amplifying genomic DNA with primers EKS191/S65.

Strain KD186 (-13 ΔC *CC3617** promoter revertant) was cloned by Gibson assembly. The wild-type *CC3617* promoter was PCR amplified from SDM1 genomic DNA with primers EK995/996. Plasmid pNPTS138 was amplified with primers EK897/898. The assembled plasmid (pKD165) was electroporated into KD170 followed by selection on PYE-kanamycin plates. An individual colony was grown overnight in PYE

and streaked onto PYE-3% sucrose plates. Colonies were screened by amplifying genomic DNA with primers EKS191/759 and Sanger sequencing.

Strain KD146 (SDM2; P*xylX-CC3617*) was produced by electroporating plasmid pEK195 into SDM2. Plasmid pEK195 was constructed by PCR-amplifying *CC3617* using primers EK739/740 and ligating into the NdeI/NheI site of pXYFPC-5.

Strain KD152 (SDM2; P*xylX-CC3617-FLAG* was produced by electroporating plasmid pEK195 into SDM2. Plasmid pEK195 was constructed by PCR-amplifying *CC3617* using primers EK879/880 and ligating into the NdeI/NheI site of pXYFPC-5.

Strain KD153 (SDM2; P*xylX-yihS-FLAG*) was produced by electroporating plasmid pEK196 into SDM2. Plasmid pEK196 was constructed by PCR-amplifying *yihS* from *E. coli* genomic DNA using primers EK751/752 and ligating into the NdeI/NheI site of pXYFPC-5. A FLAG-tag was inserted by inverse-PCR of the resulting plasmid with primers EK817/818.

Strain EK266 (SDM2; P*xylX-rffE-FLAG*) was produced by electroporating plasmid pEK260 into SDM2. Plasmid pEK260 was constructed by PCR-amplifying *rffE* from *E. coli* genomic DNA using primers EK884/885 and ligating into the NdeI/NheI site of pXCHYC-5.

Strain EK270 (SDM1; P*xylX-nanE-FLAG*) was produced by electroporating plasmid pEK264 into SDM1. Plasmid pEK264 was constructed by Gibson assembly. *nanE* was PCR-amplified from *E. coli* genomic DNA using primers EK935/936 and pXCHYC-5 was amplified with primers EK921/922.

Strain KD152 (SDM2; P*xylX*-*CC3617*-*FLAG*) was produced by electroporating plasmid pEK195 into SDM2. Plasmid pEK195 was constructed by Gibson assembly. *pmI* was PCR-amplified from *E. coli* genomic DNA using primers EK933/934 and pXCHYC-5 was amplified with primers EK921/922.

Strain KD178 (SDM2; P*xylX*::*relA* (N-terminal domain)-*FLAG*) was produced by electroporating plasmid P*xylX*::*relA* (N-terminal domain)-*FLAG* into SDM2. Plasmid P*xylX*::*relA* (N-terminal domain)-*FLAG* was constructed by PCR-amplifying the N-terminal domain of *relA* from *E. coli* genomic DNA using primers EK1085/1086 and ligating into the NdeI/NheI site of pXCHYC-5.

Table 1. Strains used in this study.

Strain	Genotype	Construction	Source
Caulobacter crescentus			
CB15	Wild-type *Caulobacter* strain CB15		(1)
NA1000	Synchronizable variant of wild-type *Caulobacter* strain CB15		(2)
KD80	Stalk-deficient mutant-1 (SDM1)	NTG-mutagenesis screen	This study
KD9	SDM1 + cosmid 2G12	Conjugation of cosmid 2G12 into SDM1	This study
KD10	SDM1 + cosmid 2H1	Conjugation of cosmid 2H1 into SDM1	This study
KD64	SDM1, P*xyl*::*CC3617*	Transformation of SDM1 with plasmid	This study
KD146	SDM2, P*xylX*::*CC3617*	Transformation of SDM2 with plasmid	This study
KD152	SDM2, P*xylX*::*CC3617-FLAG*	Transformation of SDM2 with plasmid	This study
KD145	*CC3617*::$CC3617^{A23T/G339N}$ (SDM2)	Transformation of NA1000 with plasmid and sucrose selection	This study
KD174	*CC3617*::$CC3617^{A23T}$	Transformation of NA1000 with plasmid and sucrose selection	This study
KD175	*CC3617*::$CC3617^{G339N}$	Transformation of NA1000 with plasmid and sucrose selection	This study
KD153	SDM2 + P*xylX*::*yihS-FLAG*	Transformation of SDM2 with plasmid	This study
EK203	SDM2 + P*xylX*::*yihS-FLAG* (codon-optimized)	Transformation of SDM2 with plasmid	This study
EK266	SDM2 + P*xylX*::*rffE-FLAG*	Transformation of SDM2 with plasmid	This study

EK270	SDM2 + P*xylX*::*nanE-FLAG*	Transformation of SDM2 with plasmid	This study
KD154	SDM2 + P*xylX*::*CC3617-FLAG*	Transformation of SDM2 with plasmid	This study
KD160	*CC3617*::*CC3617-mCherry*	Transformation of NA1000 with plasmid and sucrose selection	This study
KD161	*CC3617**::*CC3617*-mCherry*	Transformation of SDM2 with plasmid and sucrose selection	This study
KD170	-13 ΔC *CC3617** promoter	Suppressor screen for recovery of stalk elongation	This study
KD162	-13 ΔC *CC3617** promoter; *CC3617**::*CC3617*-mCherry*	Transformation of strain KD170 with plasmid and sucrose selection	This study
KD186	-13 ΔC *CC3617** promoter revertant	Transformation of strain KD170 with plasmid and sucrose selection	This study
KD178	*CC3617** + P*xylX*::*relA* (N-terminal domain)-*FLAG*	Transformation of CC3617* with plasmid	This study
KD181	*NA1000,* Δ*spdR*	Transformation of SDM2 with plasmid and sucrose selection	This study
EK717	MGE (mobile-genetic element)	Transformation of NA1000 with plasmid and sucrose selection	(3)
E. coli			
S17-1	λ–pir cloning strain, $Spec^R$		(4)
2G12	*C.crescentus* genomic cosmid 2G12		(5)
2H1	*C.crescentus* genomic cosmid 2H1		(5)
KD148	*BL21,* protein expression		(7)

Table 2.) Plasmids used in this study:

Name	Description	Source
pNPTS138	*sacB*-containing suicide vector used for double homologous recombination, Kan^R	Alley, M.R.K. (unpublished)
pXCHYC-5	Xylose-inducible expression, Tet^R	(6)
pKD147	His-tagged, IPTG induced expression	(8)
pKD144	pXCHYC-5-based plasmid for *CC3617* expression, Tet^R	This study
pKD186	pNPTS138-based plasmid to introduce $CC3617^{A23T/G339N}$ at the chromosomal locus, Kan^R	This study
pKD184	pNPTS138-based plasmid to introduce $CC3617^{A23T}$ at the chromosomal locus, Kan^R	This study
pKD185	pNPTS138-based plasmid to introduce $CC3617^{G339N}$ at the chromosomal locus, Kan^R	This study
pEK195	pXCHYC-5-based plasmid for *CC3617-FLAG* expression, Tet^R	This study
pEK196	pXCHYC-5-based plasmid for *yihS-FLAG* expression, Tet^R	This study
pEK228	pXCHYC-5-based plasmid for *yihS-FLAG* expression, codon optimized, Tet^R	Synthesized by GenScript, this study
pEK260	pXCHYC-5-based plasmid for *rffE-FLAG* expression, Tet^R	This study
pEK264	pXCHYC-5-based plasmid for *nanE-FLAG* expression, Tet^R	This study
pKD152	pXCHYC-5-based plasmid for *CC3617-FLAG* expression, Tet^R	This study
pKD158	pNPTS138-based plasmid to introduce a C-terminal mCherry fusion at the chromosomal *CC3617* locus, Kan^R	This study
pKD159	pNPTS138-based plasmid to introduce a C-terminal mCherry fusion at the chromosomal $CC3617^*$ locus, Kan^R	This study
pKD165	pNPTS138-based plasmid to introduce reintroduce the deleted -13 ΔC in the $CC3617^*$ suppressor strain, Kan^R	This study
pKD187	pXCHYC-5-based plasmid for *relA* (N-terminal domain)-*FLAG* expression, Tet^R	This study
pKD176	pNPTS138-based plasmid to introduce ΔspdR	This study
pKD149	pET28a plasmid to express his-tagged protein, *CC3617*, Kan^R	This study

pKD150	pET28a plasmid to express his-tagged protein, RffE, Kan^R	This study
pKD151	pET28a plasmid to express his-tagged protein, RffD, Kan^R	This study

Table 3. Primers used in this study.

Name	Sequence
Cloning primers	
EK739	tactcatATGACCAACGCTTTCGCCGA
EK740	tacttctagaTCACGAAGCCGCGTTGATCA
EK742	aCCTGATGGCCTATCTGCGCA
EK743	CCTCAGCGGCGGCGGCGG
EK751	tactcatatgAAATGGTTTAACACCCTAAGCCACAAC
EK752	tactgctagcTTATTTCGCATTAATATCCAGCAGACCCGC
EK758	tactaagcttAGGTCGCAGACCCCATTC
EK761	tactgaattcACGGCTCGTCCAATGTTCT
EK817	gactacaaggatgacgatgacaagTAAgctagctgcagcccgg
EK818	TTTCGCATTAATATCCAGCAGACCCGC
EK879	tactcatATGGAGCCTCCGATGACCAA
EK880	tactgctagcTCActtgtcatcgtcatccttgtagtcCGAAGCCGCGTTGATCACC
EK884	tactcatATGAAAGTACTGACTGTATTTGGTACGCG
EK885	tactgctagcTCActtgtcatcgtcatccttgtagtcTAGTGATATCCGATTATTTTTTAACGCTTCCAGA
EK887	GAAGACCTGGaCGGTCGAGGCG
EK888	AGGCGGTCGCGAAGTCGG
EK897	AAGCTTGGCGCCAGCCGG
EK898	GAATTCGCTAGCTTCGGC
EK921	GCTAGCTGCAGCCCGGGG
EK922	ATGGTCGTCTCCCCAAAAC
EK933	tggggagacgaccatATGCAAAAACTCATTAACTC
EK934	cgggctgcagctagcTTActtgtcatcgtcatccttgtagtcCAGCTTGTTGTAAACAC
EK935	tggggagacgaccatATGTCGTTACTTGCACAAC
EK936	cgggctgcagctagcTTActtgtcatcgtcatccttgtagtcTAGCACCGCCTTTTTC
EK985	agccggctggcgccaagcttTCCGTGAGTTCTTCGACC
EK986	tcgaattctcCGAAGCCGCGTTGATCAC
EK987	cgcggcttcgGAGAATTCGAACGTTACG
EK988	accttgctggTTACTTGTACAGCTCGTC
EK989	gtacaagtaaCCAGCAAGGTCGCCGCCC
EK990	cggccgaagctagcgaattcCTGCGGCGTTCGCCTGGTC
EK995	gctggcgccaagcttAGGTCGCAGACCCCATTC
EK996	cgaagctagcgaattcTGCATGTGCGGATTGGAC
EK1085	tactcatATGGTTGCGGTAAGAAGTGCAC
EK1086	tactgctagcttatttatcatcatcatctttataatccatGCCCATCTGCAGCTGGTAGG
Primers for assessing chromosomal point mutants	
EKS188	GCCAGATCCGTGAGTTCTTC
EK740	tacttctagaTCACGAAGCCGCGTTGATCA
EKS191	GATCGTGAACATAGCCGTGA
EKQ42R	CGATAGGCGGACAGGAAGTA
EK759	GTTTCGTCGGACCGCCCAGGTCTTCAG

QPCR Primers	Forward	Reverse

rpoH	GAGAGCGAGTGGCAGGACT	CTCTTCCAGAAGCGACATCC
cspD	CAGGCGATATCTTCGTGCAT	CGACAACCAGTCCCTTGG
katG	CCGACCTCTATGTGCTGGTC	GACCCCAGTACAGCTCTTCG
spdR	CGCATGCTGTTCTGGACAT	GTTGCCATAGCCCGTCAG

Results:

Gene CC3617 plays a critical role in stalk elongation:

To identify genes involved in stalk biosynthesis, stalk-deficient mutants were generated previously by exposing wild-type *Caulobacter* to a chemical mutagen. Stalk-deficient mutants were isolated via centrifugation and were subsequently sequenced for study. Chemical mutagenesis randomly introduces genome-wide single-nucleotide polymorphisms (SNPs) that can mildly alter, diminish or completely eliminate functionality of genes. This method is favorable over transposon mutagenesis when trying to examine functionality of both essential and nonessential genes, as transposon insertion primarily inactivates affected genes, rendering essential gene perturbations nonviable. The mutant that became the focus of the research exhibits normal stalk genesis after cell division; however, it shows a dramatically depreciated response to the well-characterized phenomenon of extreme stalk elongation upon phosphate starvation. The mutant, which will hereafter be referred to as SDM1 (stalk-deficient mutant 1), also exhibits a shorter, stubbly phase-bright cell body when starved for phosphate; however, SDM1 grows and appears indistinguishable from wild-type cells when grown in high phosphate conditions (Figure 8). This indicated that the gene or genes effected were specifically involved in the characteristic nutrient-dependent morphological differentiation of *Caulobacter*.

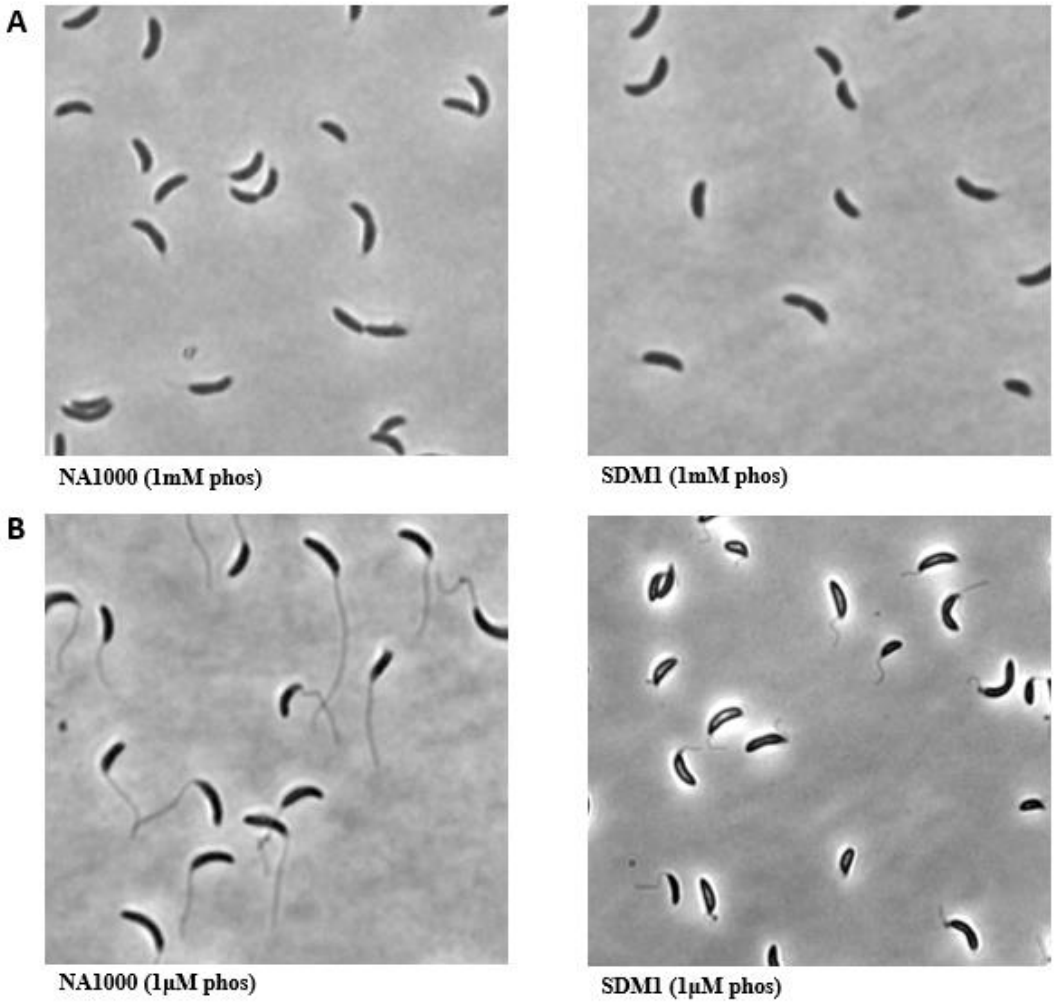

Figure. 8) (A) Wild-type and Stalk-deficient mutant 1 (SDM1) cells grown in phosphate starved media HIGG 1mM phosphate and (B) HIGG 1μM phosphate

Mutations involved in stalk malfunction were mapped via genetic complementation. A wild-type *Caulobacter* genomic library comprised of cosmids - large hybrid plasmids containing lambda phage cos sites - was used to systematically complement regions of the genome (~45kb) and cells were observed for stalk function recovery. Two genomic fragments produced stalk recovery in SDM1. Both fragments were identified to possess sequence homology of a region containing 10 genes. Out of the 10 genes shared by the genomic fragments, only a single gene, CC3617, contained mutations

in the SDM1 genome (Figure 9). Wild-type CC3617 was cloned under a xylose-inducible promoter and expressed in SDM1 cells. This yielded full recovery of wild-type stalk function in mutant cells, confirming CC3617 as being the gene responsible for stalk recovery in the initial cosmid screens. Furthermore, the mutant copy of CC3617* was selectively recombined into wild-type *Caulobacter* , creating a wild-type strain containing only the mutant CC3617* gene variant, in order to test whether CC3617 was causing stalk malfunction independently or synergistically with other mutations. NA1000::CC3617* cells showed stalk malfunction and characteristic mutant phenotype, showing that perturbation of CC3617 alone accounts for observed mutant characteristics observed in SDM1. The NA1000::CC3617* strain, referred to as SDM2, was used for all future experiments to examine the effects of CC3617 perturbation (Figure 10).

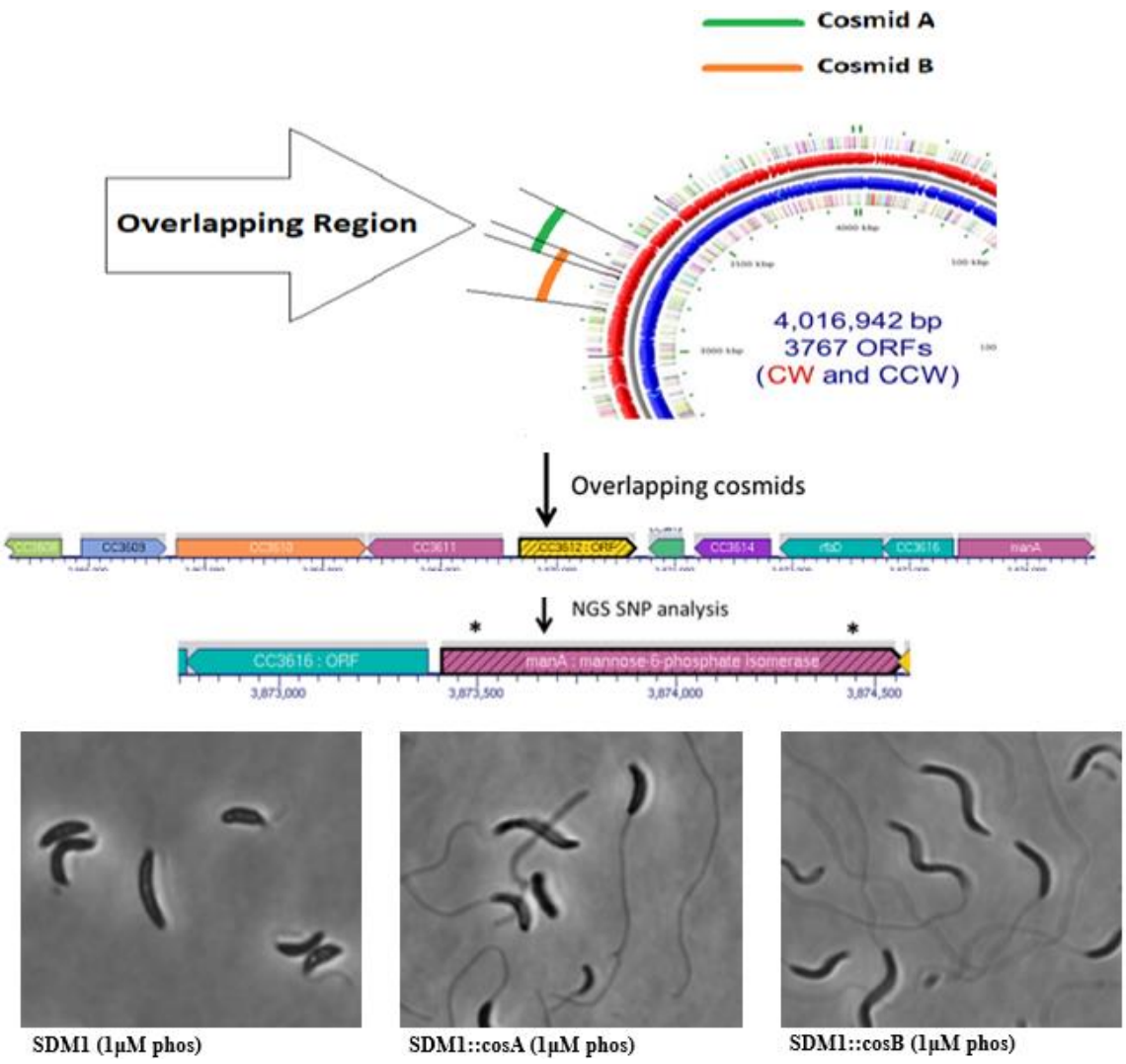

Figure. 9) Cosmid complementation of SDM1 yielded stalk elongation recovery with two genomic fragments. Both cosmid fragments shared a region of homology that contained 10 genes. Gene CC_3617(manA) was the only ORF in the mutant that possessed mutational changes.

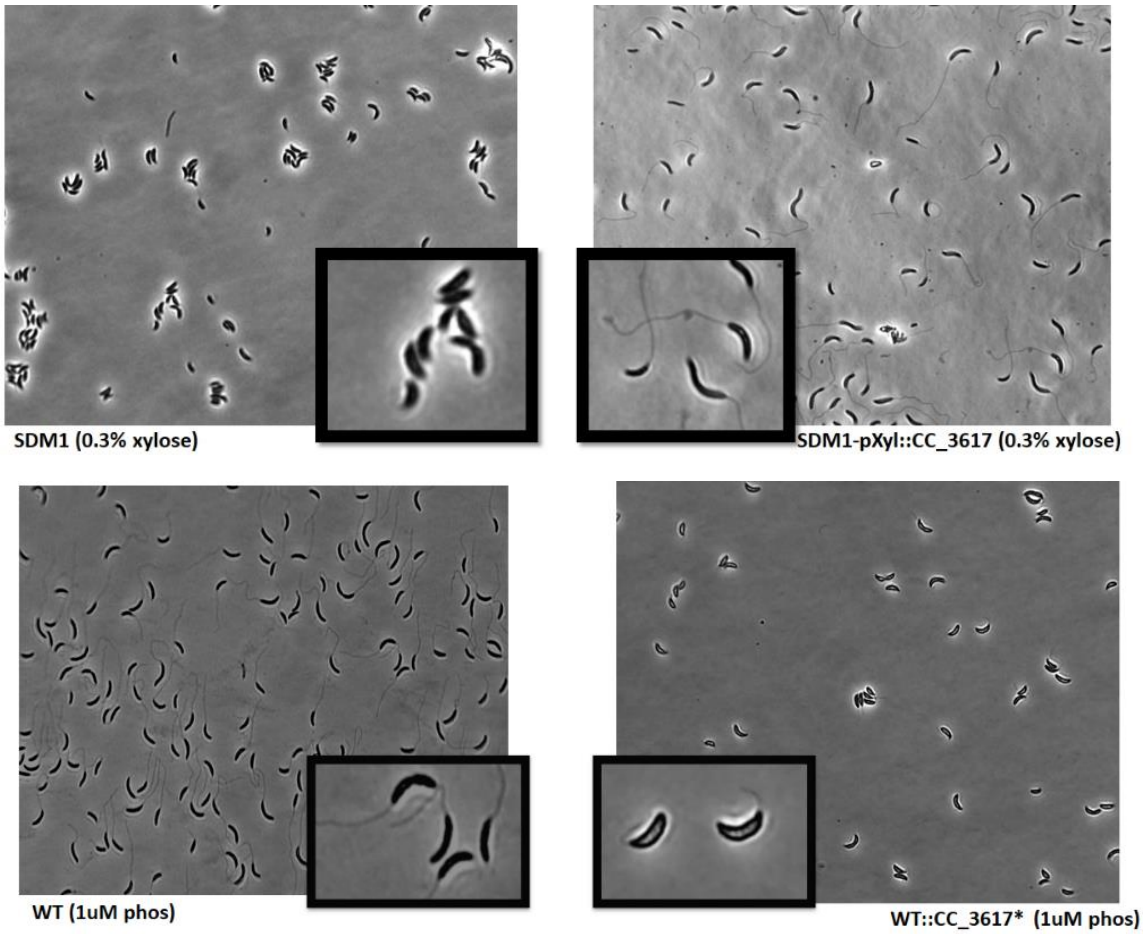

Figure. 10) Expression of functional CC3617 under a xylose-inducible promoter yielded stalk recovery in SDM1. Inversely, selective recombination yielded NA1000 cells with mutant CC3617 gene copy, resulting in stalk-deficient phenotype.*

CC3617 is a mannose-6-phosphate isomerase:

CC3617 was annotated as a N-acyl-D-glucosamine 2-epimerase in *Caulobacter* lab strain NA1000 and alternatively as a mannose-6-phosphate isomerase in strain CB15. BLAST results indicated that CC3617 shares the greatest sequence homology with the *E. coli* homolog, YihS, which is experimentally verified as a mannose isomerase. In order to ascertain the enzymatic function of CC3617, several *E. coli* homologs with experimentally-confirmed enzyme activity were expressed in SDM2 cells and examined for stalk recovery.

No recovery was observed in SDM2::YihS cells; however, recovery was observed upon expression of *E. coli* phosphomannose isomerase (PMI), despite sharing significantly less homology with CC3617 (Figure 11). *E. coli* gene encodes a mannose-6-phosphate isomerase. CC3617 was column purified and an enzyme assay confirmed mannose-6-phosphate isomerase activity. Mutant CC3617 proved incapable of being purified and was unable to be directly tested for comparison to wild-type (Figure 11). Mutant CC3617 contains two SNPs resulting in missense mutations in the form of amino acid substitutions A23T and G339D. Interestingly, these amino acids are not contained within the expected catalytic active site of the protein.

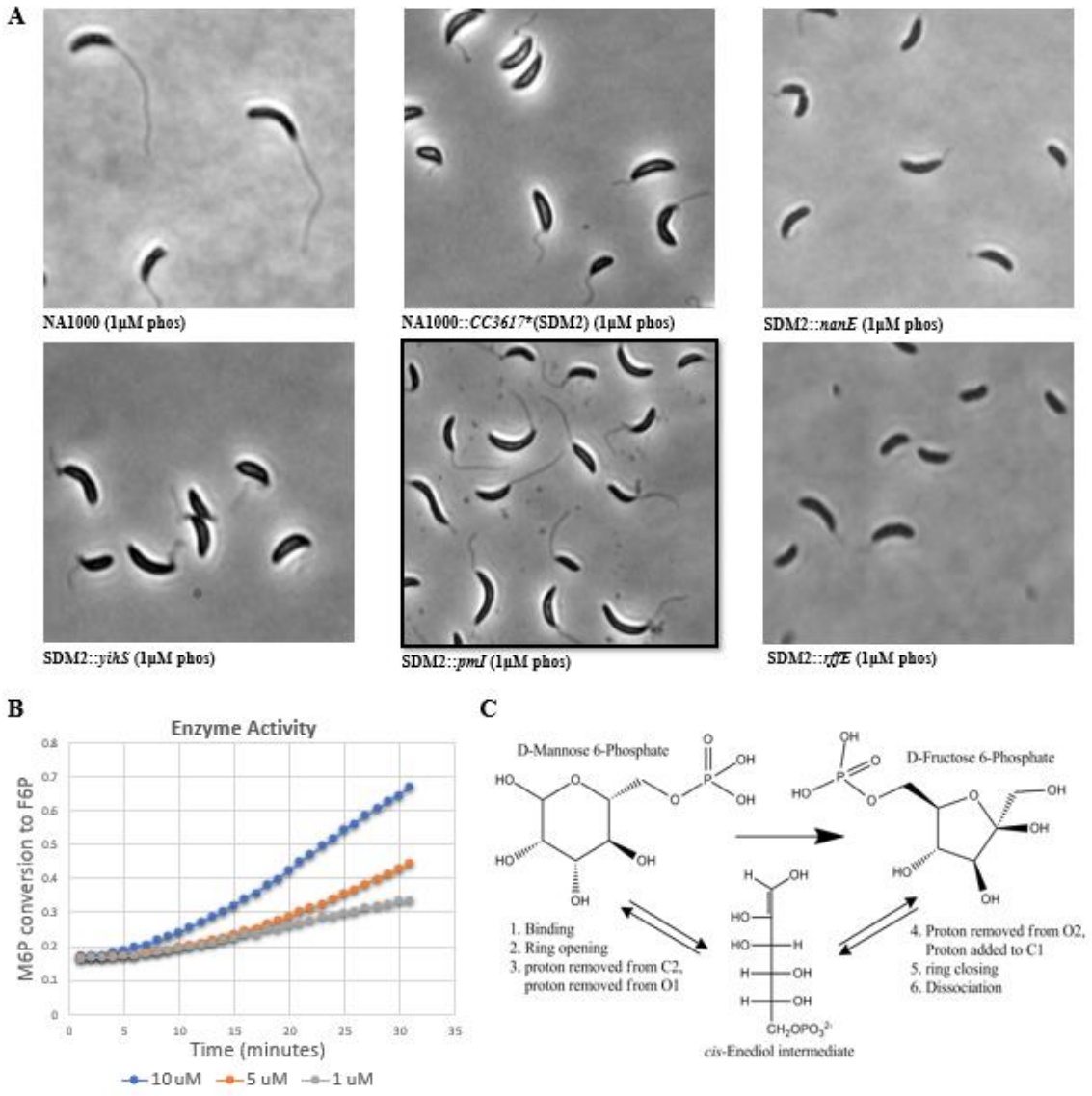

Figure. 11) (A) Exogenous expression of genes nanE, rffE, yihS and pmI in SDM2 cells. (B) Enzyme activity of purified CC3617 converting M6P into F6P. (C) Diagram of M6P isomerase enzymatic function.

Both SNPs needed to create full stalk-deficient phenotype:

In order to further assess the effect of the two point mutations (A23T and G339D) in *CC3617** and to better understand which, if not both, of the SNPs was the main causative driver of stalk deficiency, *CC3617* gene copies with each of the individual SNPs were created and selectively recombined into NA1000. The single SNP mutants were grown in

low phosphate and stalk lengths were compared to NA1000 and SDM2 (Figure 12). The results showed that, although the 3' SNP had the greatest contribution to stalk deficiency, both SNPs were in fact needed to achieve the phenotype observed in SDM2 cells. It would seem that both SNPs have a synergistic effect increasing the overall intensity of *CC3617* perturbation.

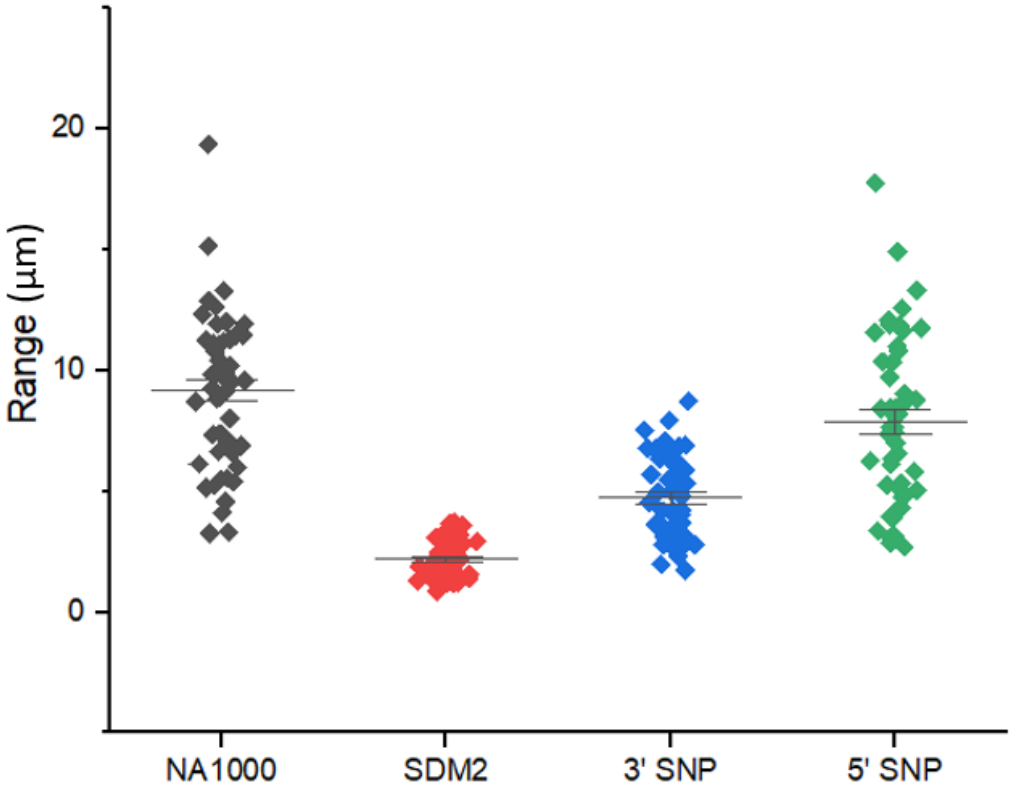

Figure. 12) Stalk measurements taken after 72 hours in HIGG 1µM phosphate. All data sets are P<0.001

Suppressor mutant exhibits stalk recovery with high CC3617* expression:

A suppressor mutation screen was used to isolate gain-of-function mutants to shed light on the nature of CC3617 perturbation, and why it affects stalk elongation, by generating a new mutation that can counteract the original. Screens yielded an SDM2

mutant that responded to phosphate starvation with proper stalk elongation and appeared fully wild-type in nature. Upon sequencing the mutant, it was discovered that the mutant CC3617* gene copy was retained; however, a single cytosine deletion upstream of the CC3617* ORF (-13 from the transcription start site) was newly present, indicating a possible alteration of RBS or promoter region activity. qRT-PCR revealed that the C deletion was driving an ~80 fold induction increase of CC3617*. Additionally, fluorescent protein fusions revealed that the high expression level carries over to the protein level, showing super high protein abundance in both high and low phosphate conditions (Figure 13). This showed that SDM2 mutant phenotype could be overcome with massive overexpression of CC3617*, indicating that the mutant protein does exhibit M6P isomerase activity but at either a much lower efficiency, or possibly reduced in abundance through an aggregation effect. This theory may also explain the inability to purify the mutant protein as it may form aggregates with other proteins or each other. This may also explain the apparent reduction in physiological function of CC3617 despite having mutations not located in the catalytic site. Perhaps the amino acid substitutions create a ‘sticky’ region of the protein that interacts and associates with other CC3617 proteins or possibly other proteins altogether. It may also be that mutant CC3617* gets packaged into inclusion bodies; however, fluorescently-tagged CC3617* does not appear to be confined to inclusion bodies in microscopy imaging. CC3617 exhibits no visible site of localization in the cell and is diffuse in both wild-type and SDM2 cells.

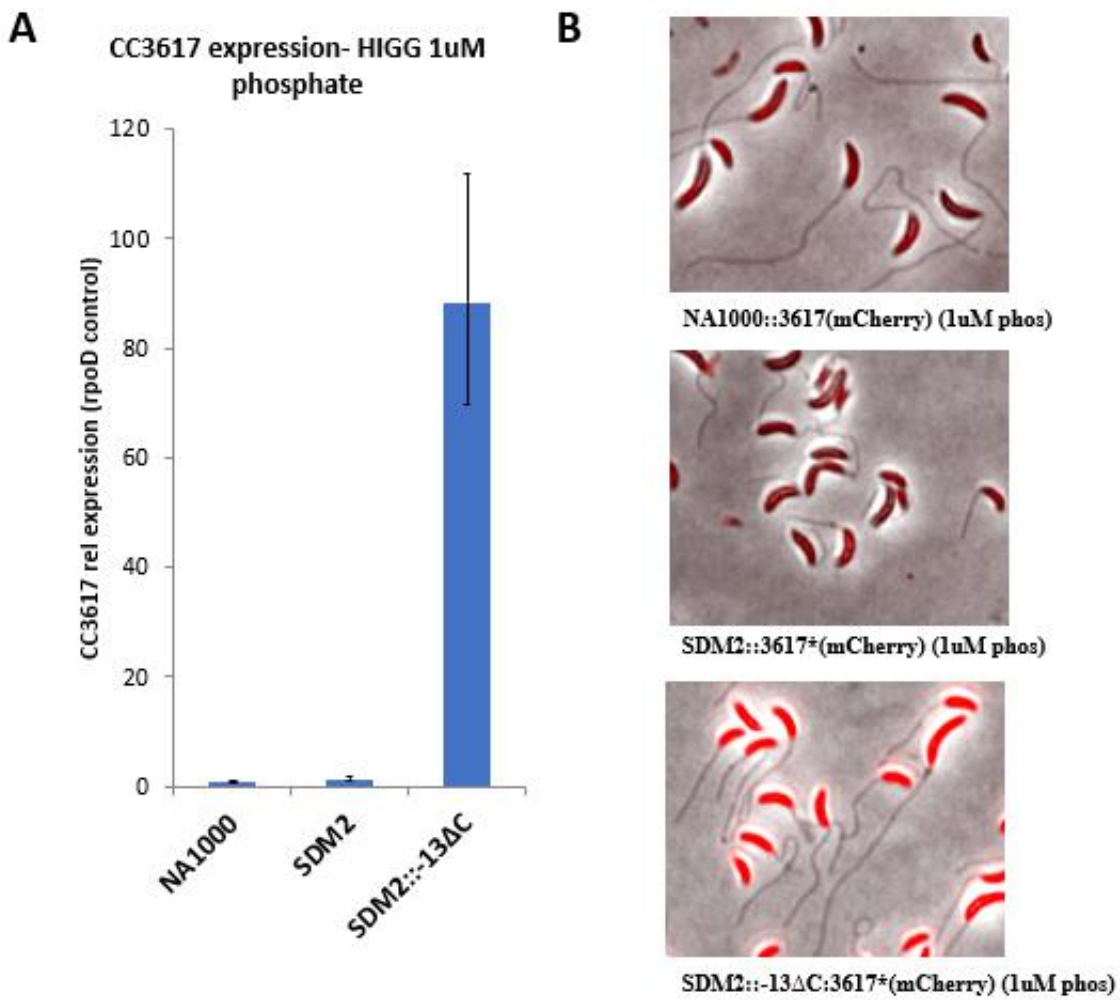

Figure. 13) (A) CC3617 fold induction upon phosphate starvation in NA1000, SDM2 and SDM2::-13ΔC(suppressor mutant) showing ~80 fold increase in expression over NA1000 and SDM2. (B) Microscopy images of cells with CC3617(mCherry) showing much higher abundance of CC3617 expressed in suppressor mutant cells.

Sugar phosphate metabolic flux during phosphate starvation:

CC3617 was confirmed to interconvert mannose-6-phosphate and fructose-6-phosphate; however, it was unclear how such a sugar metabolism perturbation would affect stalk elongation while largely leaving many properties of the cell unaffected. More interestingly, qRT-PCR results show that both wild-type and SDM2 exhibit similar

increases of expression levels of CC3617 in low phosphate conditions (figure 17). This indicated that the stalk deficiency was likely a result of a metabolic disruption and not directly linked to gene regulation. Alterations in metabolism were examined via metabolomic analyses on wild-type and SDM2 cells in both phosphate-replete and phosphate starved-conditions. The data indicates that wild-type *Caulobacter* maintain an equilibrium between M6P and F6P in either phosphate abundance or depletion; however, upon phosphate starvation, it was observed that SDM2 lost equilibrium between the sugars and became F6P dominant, becoming approximately twice as abundant (Figure 14). This indicated that during phosphate starvation the differentiation *Caulobacter* undergoes results in either a reduction of F6P consumption, an increase in M6P consumption or both, and that the proper flux of these metabolites is critical to either supplying essential materials or signaling to the cell about the current nutritional climate via cytoplasmic abundance. In addition to M6P and F6P, multiple glycolysis and TCA cycle metabolites were found to be reduced while NTPs were increased in abundance (Figure 14).

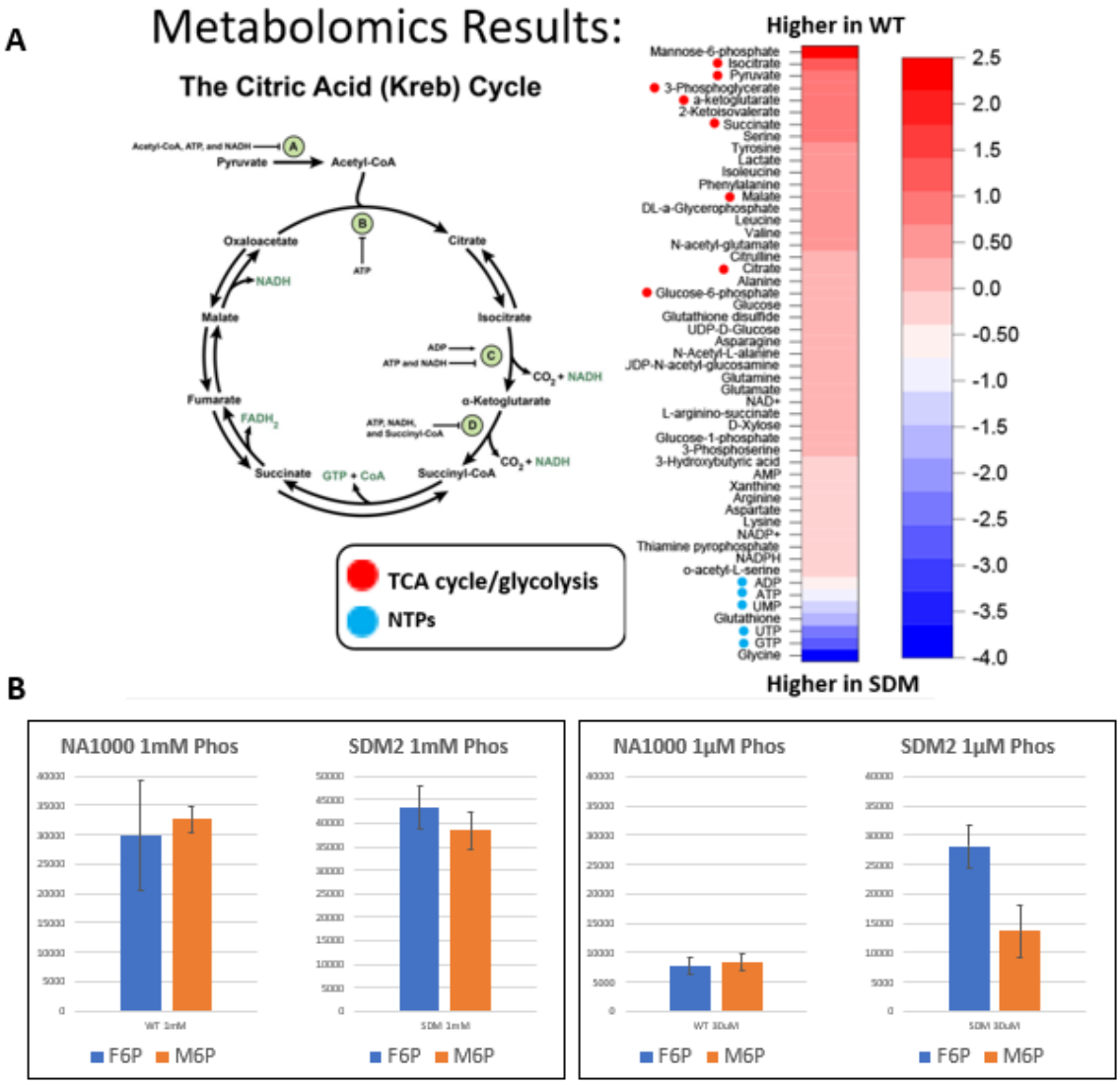

Figure. 14) (A) Metabolomic data showing the accumulation of TCA cycle metabolites in NA1000 upon phosphate starvation. (B) Metabolomic data showing relative abundance of F6P and M6P in high and low phosphate conditions.

Characterization of CC3617 physiological function:

M6P and F6P are important molecular precursors for energy production and structural molecules of the cell envelope. In order to see whether CC3617* perturbation was structurally compromising the cell or involved strictly in a signaling event, preliminary stress tests were performed to deduce cellular integrity. Wild-type and SDM2 cells were

grown in a variety of toxins and antibiotics including tetracycline, vancomycin, bacitracin, SDS and zinc sulfate (Figure 15). Antibiotics like vancomycin and bacitracin affect cell wall production, and due to their membrane impermeability, are intrinsically weak against gram-negative bacteria, making them useful in determining defective outer membrane integrity. Stress test results indicated that SDM2 cells were more susceptible to vancomycin and bacitracin, indicating a defect of the outer membrane.

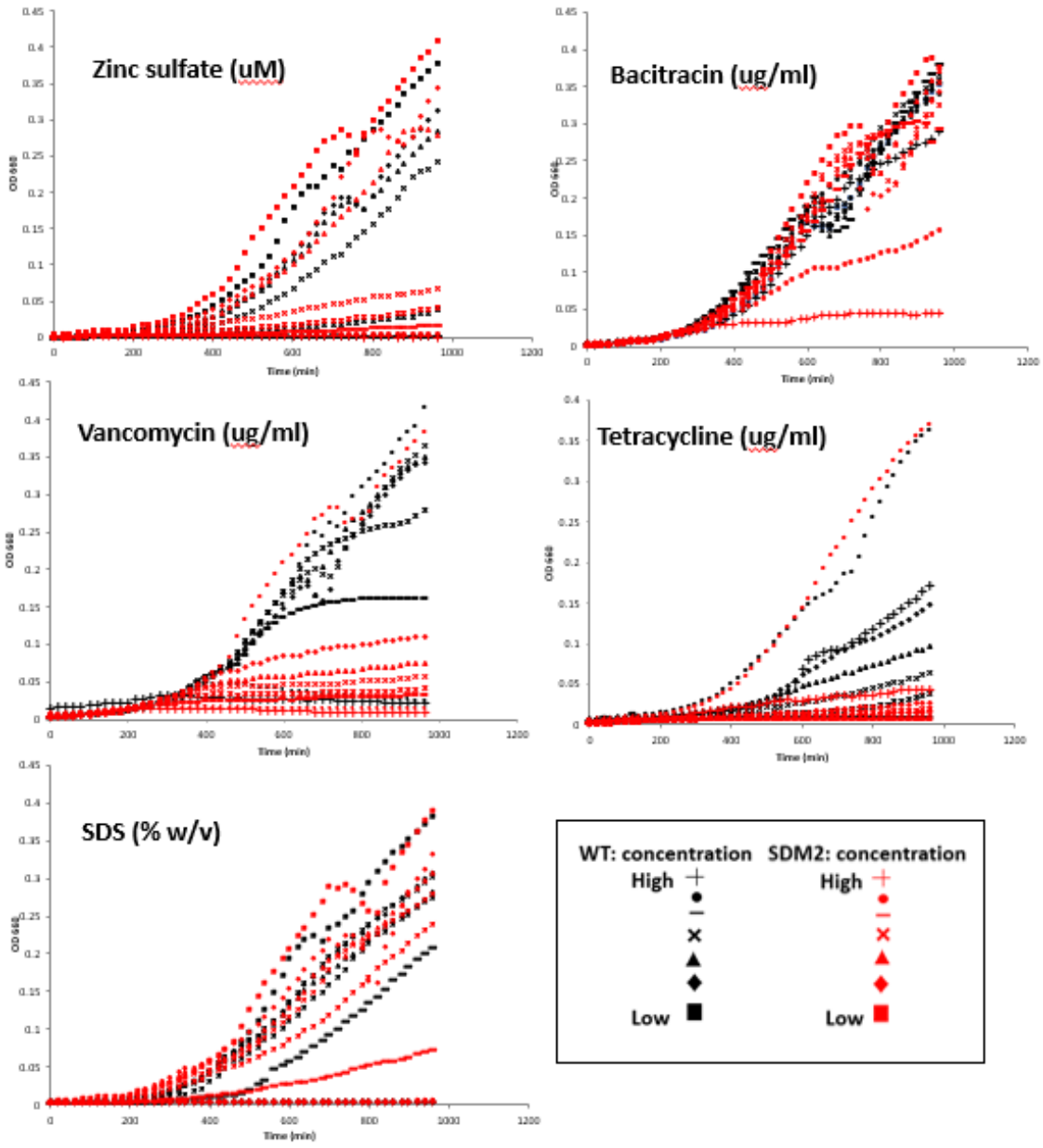

Figure. 15) NA1000 and SDM2 were grown in HIGG 1μM with various concentrations of bacterial toxins: SDS, tetracycline, bacitracin, vancomycin, zinc sulfate. Growth was measured over a 16-hour period.

In order to identify which components of the cell envelope were altered in SDM2, multiple cell materials known to be synthesized by M6P- and F6P-derived precursors were tested to find physiological effects of CC3617* perturbation (Figure 16). Bacterial cell walls are an encapsulating polymer matrix composed of peptidoglycan (PG) that sits in the periplasm between the outer and inner membranes. Additionally, peptidoglycan is synthesized primarily from F6P-derived components. Cell wall was purified and analyzed to compare SDM2 peptidoglycan to wild-type cells. Results show no gross differences between mutant and wild-type PG, indicating that CC3617* perturbation does not interfere with proper PG synthesis. Furthermore, the formation and presence of extracellular polymeric substance (EPS), a M6P-derived mucoid substance excreted by cells to form biofilm, was examined. SDM2 was found to lack apparent EPS secretion, while wild-type (NA1000) cells exhibit abundant EPS production in the form of a slimy mucosal film produced by cell colonies.

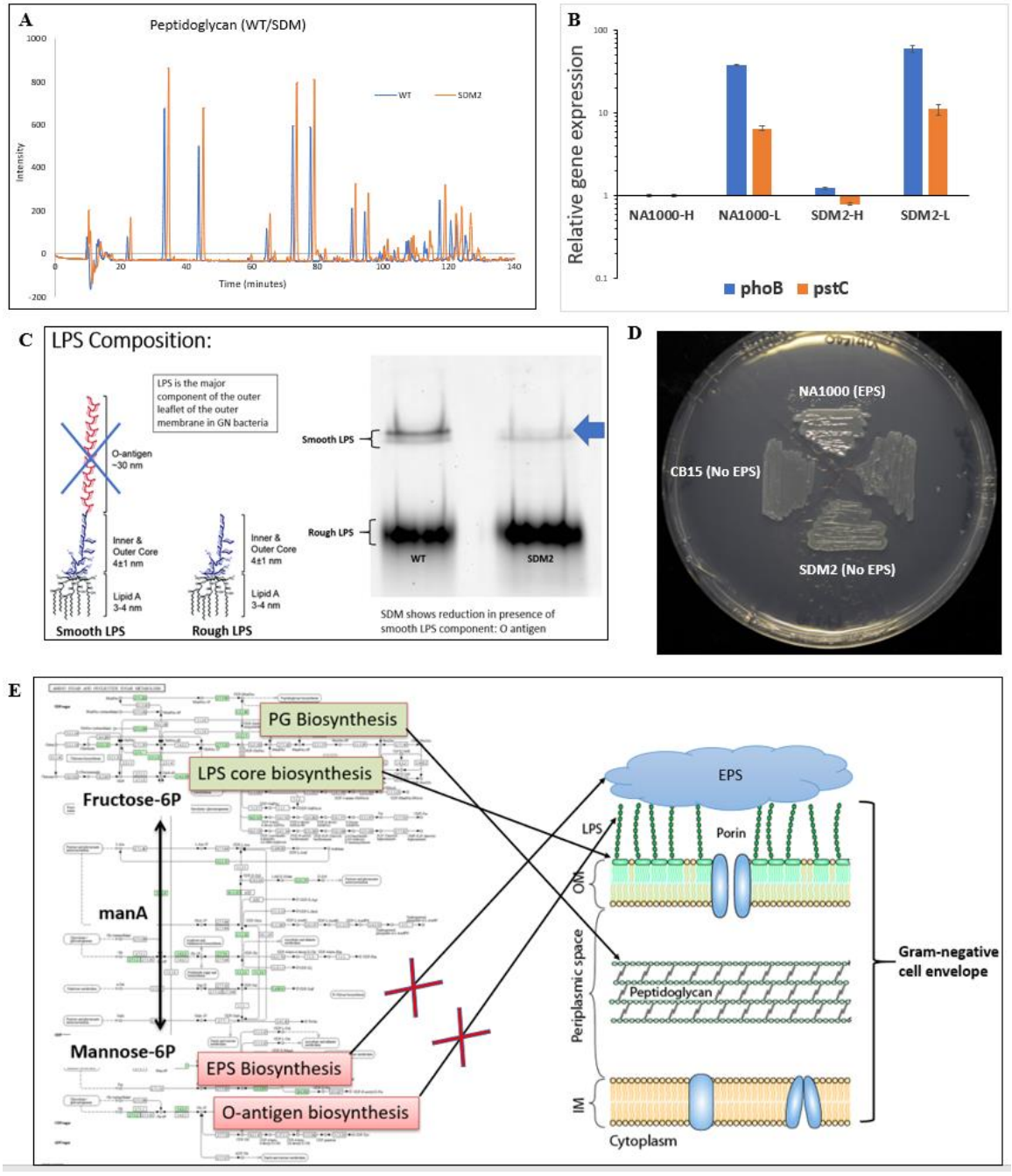

Figure. 16) (A) Mass spec of cell wall composition. Peptidoglycan composition is unaffected in SDM2 cells. (B) Expression of phosphate-induced genes (phoB and pstC) in phosphate abundance and starvation. Data shows SDM2 cells can properly sense and uptake phosphate. (C) Analysis of lipopolysaccharide composition. SDM2 is deficient in smooth-LPS species, indicative of O-antigen deficiency, while maintaining LPS core subunit. (D) Visual inspection of EPS secretion. SDM2 lacks secretion of mucoidal EPS. (E) Summary of results as they pertain to cell envelope composition.

Additionally, lipopolysaccharide composition was examined. Lipopolysaccharide (LPS) is the major component of the outer leaflet of the outer membrane of gram-negative bacteria. LPS consists of a lipid base known as lipid A, a core oligosaccharide component derived from F6P and a repetitive glycan polymer known as the O-antigen which is M6P-derived. Examination of SDM2 LPS revealed a depleted amount of "smooth-type" LPS species, which is the LPS variant possessing the O-antigen chain. This indicates that lipid A and core oligosaccharide components are adequately synthesized, but O-antigen is reduced in prevalence.

Taken collectively, these data indicate a disparity between F6P- and M6P-derived molecules; having no apparent obstruction to synthesizing F6P-derived products while showing a reduction in multiple M6P-derived components. This potentially correlates with metabolomics data which indicates a possible reduction of M6P accompanied by an accumulation of F6P in SDM2 cells in low phosphate. A possible scenario that could account for all observed phenomena would be one in which, upon phosphate starvation, M6P becomes increasingly consumed through cell processes involved in cell differentiation and stalk elongation. In such a scenario, F6P would be converted into M6P due to the shifting concentration gradient. In SDM2, interconversion between M6P and F6P would be heavily impeded, which would result in an accumulation of F6P and a depletion of M6P which cannot be supplemented via F6P conversion. Despite these observed disruptions in SDM2 physiology, it cannot be determined definitively if these are the causation for the deficiency in stalk elongation as none of the observed components lacking in SDM2 are known to be essential for cell envelope biosynthesis.

Sugar phosphate flux essential for stationary phase onset in low phosphate:

SDM2 was observed to grow to an abnormally high OD when grown beyond 72 hours in comparison to wild-type cells. In addition to visual observations, metabolomic data showed a higher level of TCA cycle metabolites in wild-type cells which corresponds with data indicating an accumulation of TCA cycle metabolites upon induction of stationary phase. Interestingly, growth curve data shows that SDM2 and wild-type cells grow similarly in high-phosphate conditions; however, SDM2 grows to a substantially higher OD in low-phosphate conditions. In order to examine this phenomenon further, expression of several genes corresponding to stationary phase were examined. c*spD*, *katG* and *spdR* are all genes heavily induced upon the onset of stationary phase. The qRT-PCR data indicated that all genes examined were greatly reduced in expression in SDM2 (Figure 17). This data indicated that SDM2 is conditionally foregoing normal stationary phase induction. It is likely that when phosphate starvation induces the onset of stalk elongation and alters the flux of sugar phosphates, it leaves SDM2 in a state of depleted M6P which would be replenished through F6P conversion in wild-type cells. M6P depletion possibly interferes with proper stationary phase onset; however, this is not yet clear.

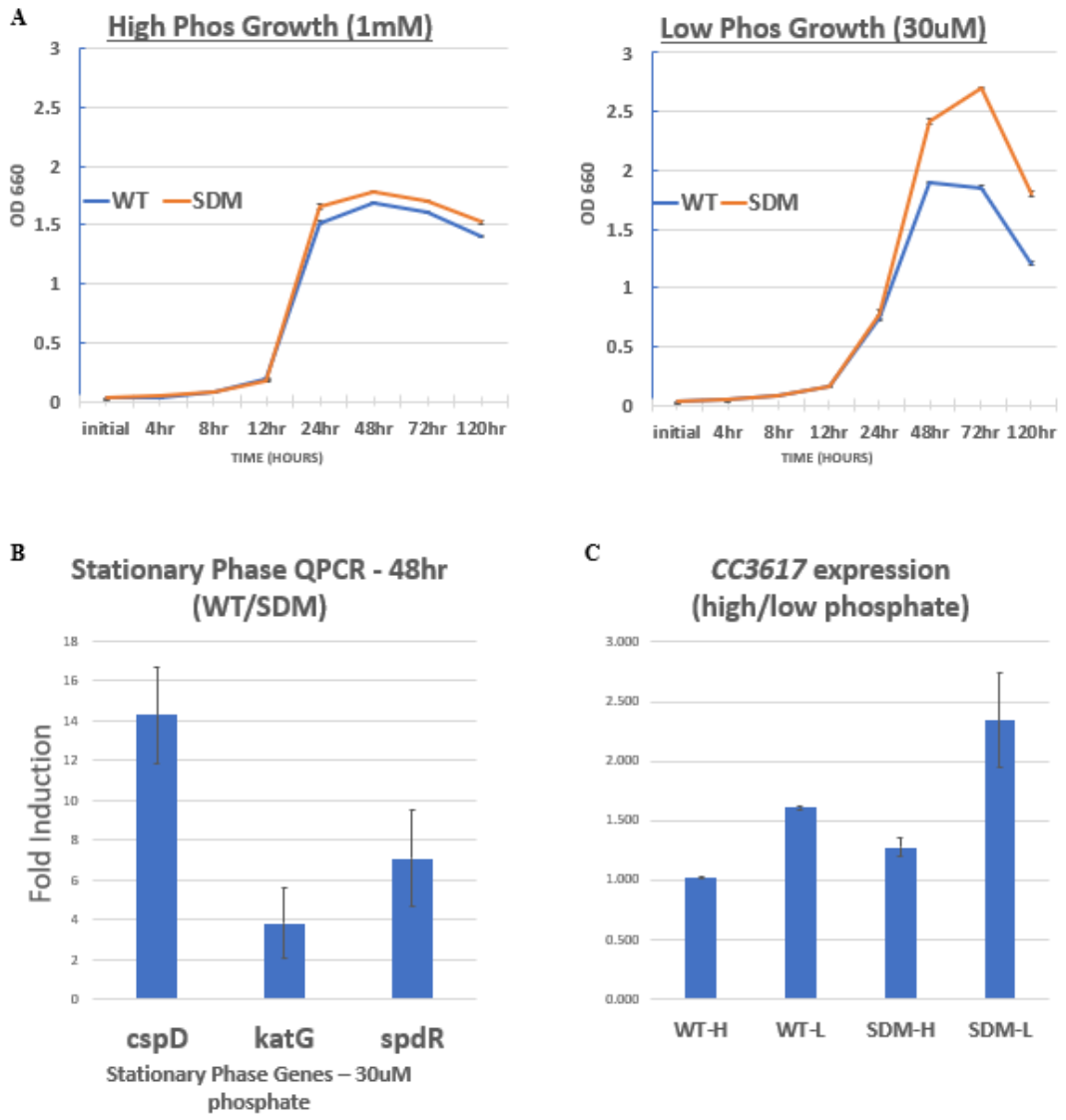

Figure. 17) (A) Growth curve data in high and low phosphate. SDM2 foregoes stationary phase differentially upon phosphate starvation. (B) Fold induction increase of NA1000 over SDM2 in low phosphate after 48 hours of stationary phase genes: cspD, katG and spdR.(C) CC3617 fold induction upon phosphate starvation.

Stationary phase stimulates stalk elongation:

In order to examine the significance of SDM2 foregoing stationary phase and lacking the ability to elongate a stalk in low phosphate conditions, an experiment was designed to artificially induce stationary phase in SDM2 cells. A constitutively active N-terminal domain truncation of *E. coli* gene, *relA*, a pyrophosphokinase that converts GTP

into the stationary phase-inducing stress hormone, ppGpp, was cloned and expressed in wild-type and SDM2 cells. *Caulobacter* also makes ppGpp via the gene *spoT*; however, it is not constitutively active, making the *E. coli relA* truncation more useful. Upon RelA expression, wild-type cells appear unchanged, while SDM2 cells exhibit a significant increase in stalk elongation. Additionally, perturbation of both *spdR* and *spoT*, genes responsible for stationary phase onset in *Caulobacter*, show a reduction in stalk elongation when compared to NA1000 cells after 24 hours (Figure 18). This would seem to indicate that stationary phase is inherently tied to cell differentiation and stalk elongation. It would also appear that the global metabolic flux of mannose-6-phosphate and fructose-6-phsophate plays a role in a specific phosphate-dependent induction of stationary phase and subsequent stalk elongation, or it is possible that the perturbation observed in SDM2 is causing a disruptive phenomenon that is differentially interfering with stationary phase onset under phosphate starved conditions.

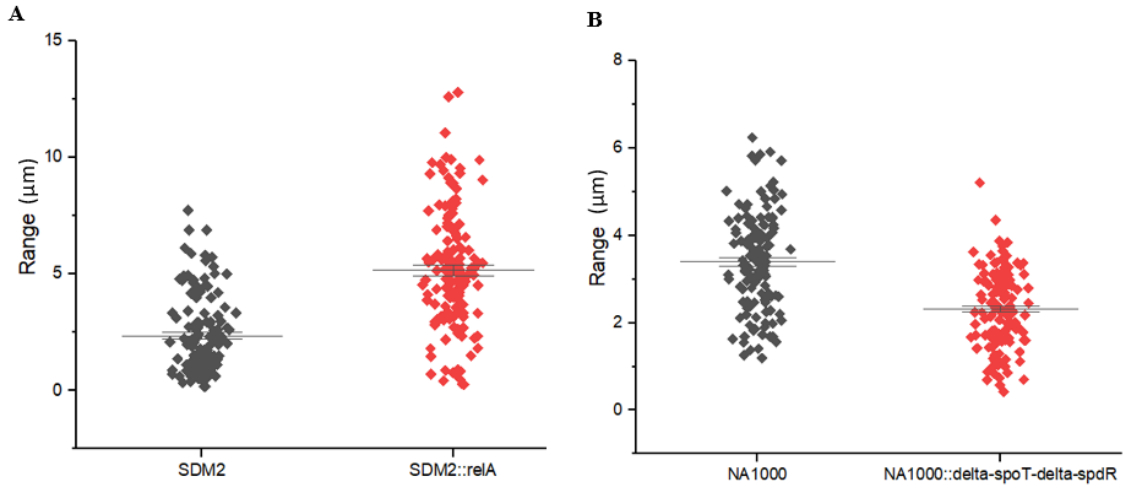

Figure.18) (A) Stalk length measurements of SDM2 and SDM upon relA expression after 96 hours of growth in HIGG 30µM. Stalk length significantly increases upon relA expression (P<0.001). (B) Stalk length measurements of NA1000 and NA1000::ΔspdR-ΔspoT after 24 hours of growth in 30µM HIGG. Deletion of stationary phase genes in NA1000 results in stalk length impediment (p<0.001).

Discussion:

Our research has uncovered a previously unknown connection between sugar phosphate metabolism and *Caulobacter* stalk elongation that is either directly or indirectly associated with stationary phase induction. Our data indicates a maintained global equilibrium between the two sugar phosphate species, M6P and F6P, irrespective of growth mode in WT *Caulobacter,* though the total pool size and metabolism of these sugar phosphates change upon growth mode transition, corroborating our observations. SDM2, which lacks a sufficiently functional M6P/F6P interconversion pathway (CC3617) shows a disparity in sugar phosphate equilibrium when starved for phosphate, with an approximate 2:1 F6P/M6P ratio observed, while still maintaining a 1:1 ratio in phosphate-replete media. Both WT *Caulobacter* and SDM2 do not exhibit any substantial changes in CC3617 expression level, protein localization or abundance when starved for phosphate, maintaining a relatively static and diffuse presence in the cell, indicating that the observed phenomenon are directly linked to differential global metabolism of M6P and F6P and not directly regulated on the genetic level regarding their interconversion.

It would appear that global metabolic demand of M6P and F6P is adjusted alternatively when transitioning to the slow-growing, stalk-forming cell growth mode triggered by phosphate starvation. The data could either indicate that during phosphate starvation, F6P increases in abundance through increased production via glucose-6-phosphate conversion or decreased metabolic consumption, or alternatively, M6P is more rapidly consumed by the changing physiological demands of stalk elongation. It is likely that the latter is true as all measured M6P-derived cell components were observed to be deficient in SDM2 under phosphate starvation while F6P components were unaffected,

indicating that M6P is being consumed too fast to be adequately replenished by F6P conversion via the perturbed mutant CC3617*. This metabolic shift is undetectable in WT *Caulobacter* using conventional metabolomic analysis because fully functional CC3617 maintains steady M6P/F6P equilibrium even as sugar phosphate demand alters upon the onset of stalk elongation.

Interestingly, Caulobacter is extremely poor at growing on fructose and mannose as a sole carbon source, showing extreme cell malformation and extremely slow growth in HIGG media with the mannose and fructose substituted for glucose (Figure 19). It is likely that the cells are only viable by utilizing the glutamate source in HIGG media as a primary carbon source. This likely accounts for CC3617 being an essential gene, whereas M6P isomerases are nonessential in other species, due to *Caulobacter* being bottle-necked into deriving all sugar phosphate species through a limited number of enzymatic starting points (Richards, et al. 2013). Additionally, all experiments were conducted using HIGG media which supplies glucose as a primary carbon source. Glucose is directly converted to Glucose-6-phosphate which can be directly converted to fructose-6-phosphate; however, *Caulobacter* possesses no enzyme to convert G6P to M6P, meaning all M6P must be derived through F6P conversion. This supports the theory that M6P demand drastically increases upon phosphate starvation, as even SDM2 can maintain M6P/F6P equilibrium in phosphate-replete media but loses equilibrium upon starvation.

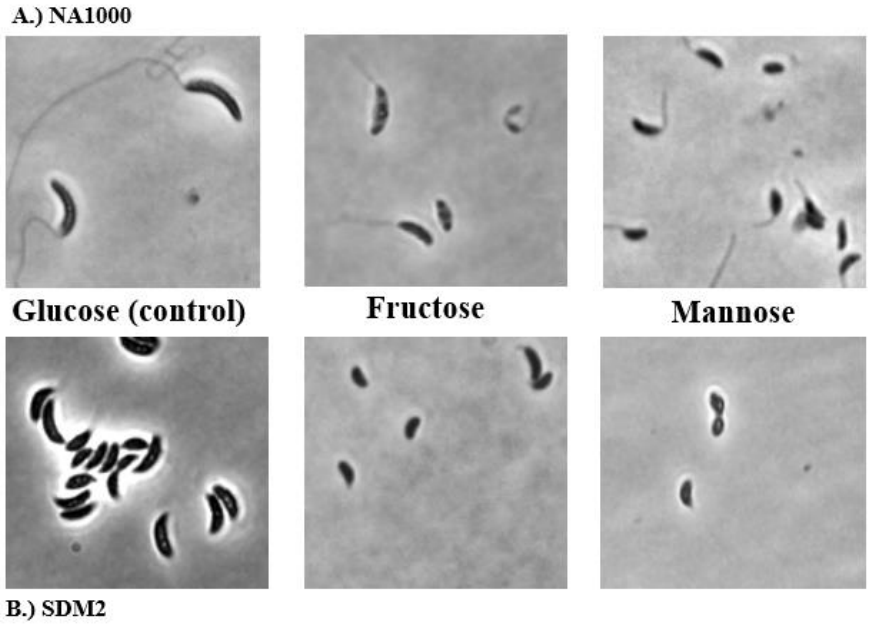

Figure. 19) NA1000 and SDM2 grown in HIGG 30μM phosphate with glucose, fructose and mannose as primary media carbon sources. Caulobacter grows poorly in fructose and mannose.

Our data cannot distinguish precisely whether F6P is accumulated or depleted during phosphate starvation as it can be readily replenished via excess G6P and there is no indication of a deficiency in the F6P-derived cell wall and LPS core production; however, it has been shown in *E. coli* that relative pool size of F6P alters growth rate, with excess F6P resulting in a growth rate reduction (Persson, et al. 2007). Our data does not distinctly correlate with this observation, but *Caulobacter* is an entirely different bacterial species altogether; however, it does corroborate that fact that sugar phosphate metabolism influences division rate. Furthermore, our data shows that SDM2 foregoes stationary phase only upon phosphate starvation and regains partial stalk functionality upon forced onset of stationary phase via RelA expression. This may be explained by a model wherein global M6P pool size directly induces or is sensed by an unknown mechanism to induce stationary phase in *Caulobacter*. In SDM2, it is possible that phosphate starvation induces stalk elongation immediately; consuming too much M6P without an efficient means of replenishing the pool size, which leads to a deficiency in stationary phase-inducing signals. It is possible that phosphate starvation initiates stalk elongation, but stationary phase

subsequently ramps up the elongation signaling significantly which aligns with our data on stationary phase knockout mutant stalk length data. It is also possible, but less likely, that inducing stationary phase slows consumption of F6P and causes an accumulation, which subsequently increases the concentration differential between M6P and F6P, increasing the conversion rate to an adequate enough level to properly feed stalk synthesis precursors.

This modification of M6P and F6P demand could be explained by alternative models based on assumptions about the two *Caulobacter* growth modes: 1.) Rapid division, short stalk growth mode demands more ATP, and subsequently more F6P than the alternate growth mode due to high energy demands for genome replication and cell division. 2.) Slow division, long stalk growth mode needs less ATP and F6P as it is readily dividing much slower; however, stalk synthesis requires a much higher demand of M6P-derived precursor molecules to produce adequate amounts of cell envelope building materials and or to properly signal for stationary phase induction. Though the exact mechanism has not yet been completely defined, several things are known in general: Perturbation of the M6P isomerase, CC3617, results in a dramatic loss of responsiveness to phosphate-dependent stalk elongation, while still maintaining the ability to initially synthesize a stalk upon flagellar shedding. Additionally, *Caulobacter* maintains an equilibrium between F6P and M6P independent of phosphate abundance. Interruption of the M6P/F6P interconversion pathway results in a break in equilibrium upon phosphate starvation, showing more F6P than M6P resulting in ~2:1 ratio. This break in equilibrium is coupled with a deficiency in M6P-derived cell envelope and extracellular components along with a suppression of stationary phase induction.

Bibliography:

Billini, Maria, Jacob Biboy, Juliane Kühn, Waldemar Vollmer, and Martin Thanbichler. "A Specialized MreB-Dependent Cell Wall Biosynthetic Complex Mediates the Formation of Stalk-Specific Peptidoglycan in Caulobacter Crescentus." PLOS Genetics 15, no. 2 (February 1, 2019): e1007897. https://doi.org/10.1371/journal.pgen.1007897.

Cabeen, Matthew T., Michelle A. Murolo, Ariane Briegel, N. Khai Bui, Waldemar Vollmer, Nora Ausmees, Grant J. Jensen, and Christine Jacobs-Wagner. "Mutations in the Lipopolysaccharide Biosynthesis Pathway Interfere with Crescentin-Mediated Cell Curvature in Caulobacter Crescentus." Journal of Bacteriology 192, no. 13 (July 1, 2010): 3368–78. https://doi.org/10.1128/JB.01371-09.

Curtis, Patrick D., and Yves V. Brun. "Getting in the Loop: Regulation of Development in Caulobacter Crescentus." Microbiol. Mol. Biol. Rev. 74, no. 1 (March 1, 2010): 13–41. https://doi.org/10.1128/MMBR.00040-09.

Desmarais, Samantha M., Felipe Cava, Miguel A. de Pedro, and Kerwyn Casey Huang. "Isolation and Preparation of Bacterial Cell Walls for Compositional Analysis by Ultra Performance Liquid Chromatography." Journal of Visualized Experiments: JoVE, no. 83 (January 15, 2014): e51183. https://doi.org/10.3791/51183.

Divakaruni, Arun V., Rachel R. Ogorzalek Loo, Yongming Xie, Joseph A. Loo, and James W. Gober. "The Cell-Shape Protein MreC Interacts with Extracytoplasmic Proteins Including Cell Wall Assembly Complexes in Caulobacter Crescentus." Proceedings of the National Academy of Sciences 102, no. 51 (December 20, 2005): 18602–7. https://doi.org/10.1073/pnas.0507937102.

Gonin, Madeleine, Ellen M. Quardokus, Danielle O'Donnol, Janine Maddock, and Yves V. Brun. "Regulation of Stalk Elongation by Phosphate InCaulobacter Crescentus." Journal of Bacteriology 182, no. 2 (January 15, 2000): 337–47. https://doi.org/10.1128/JB.182.2.337-347.2000.

Hughes, Velocity, Chao Jiang, and Yves Brun. "Caulobacter Crescentus." Current Biology 22, no. 13 (July 2012): R507–9. https://doi.org/10.1016/j.cub.2012.05.036.

Jenal, Urs. "Signal Transduction Mechanisms in Caulobacter Crescentus Development and Cell Cycle Control." FEMS Microbiology Reviews 24, no. 2 (April 1, 2000): 177–91. https://doi.org/10.1016/S0168-6445(99)00035-2.

Jeong, Haeyoung, Hyun Ju Kim, and Sang Jun Lee. "Complete Genome Sequence of Escherichia Coli Strain BL21." Genome Announcements 3, no. 2 (March 19, 2015). https://doi.org/10.1128/genomeA.00134-15.

Jones, Michael D., Evgeny Vinogradov, John F. Nomellini, and John Smit. "The Core and O-Polysaccharide Structure of the Caulobacter Crescentus Lipopolysaccharide."

Carbohydrate Research 402 (January 30, 2015): 111–17. https://doi.org/10.1016/j.carres.2014.10.003.

Klein, Eric A, Susan Schlimpert, Velocity Hughes, Yves V Brun, Martin Thanbichler, and Zemer Gitai. "Physiological Role of Stalk Lengthening in Caulobacter Crescentus." Communicative & Integrative Biology 6, no. 4 (July 1, 2013). https://doi.org/10.4161/cib.24561.

Kühn, Juliane, Ariane Briegel, Erhard Mörschel, Jörg Kahnt, Katja Leser, Stephanie Wick, Grant J. Jensen, and Martin Thanbichler. "Bactofilins, a Ubiquitous Class of Cytoskeletal Proteins Mediating Polar Localization of a Cell Wall Synthase in Caulobacter Crescentus." The EMBO Journal 29, no. 2 (January 20, 2010): 327–39. https://doi.org/10.1038/emboj.2009.358.

Lin, Lin, and Martin Thanbichler. "Nucleotide-Independent Cytoskeletal Scaffolds in Bacteria." Cytoskeleton (Hoboken, N.J.) 70, no. 8 (August 2013): 409–23. https://doi.org/10.1002/cm.21126.

Lohmiller, S., K. Hantke, S. I. Patzer, and V. Braun. "TonB-Dependent Maltose Transport by Caulobacter Crescentus." Microbiology (Reading, England) 154, no. Pt 6 (June 2008): 1748–54. https://doi.org/10.1099/mic.0.2008/017350-0.

Perez, Adam M., Thomas H. Mann, Keren Lasker, Daniel G. Ahrens, Michael R. Eckart, and Lucy Shapiro. "A Localized Complex of Two Protein Oligomers Controls the Orientation of Cell Polarity." MBio 8, no. 1 (28 2017). https://doi.org/10.1128/mBio.02238-16.

Persson, Örjan, Åsa Valadi, Thomas Nyström, and Anne Farewell. "Metabolic Control of the Escherichia Coli Universal Stress Protein Response through Fructose-6-Phosphate." Molecular Microbiology 65, no. 4 (2007): 968–78. https://doi.org/10.1111/j.1365-2958.2007.05838.x.

Richards, Gregory R., Maulik V. Patel, Chelsea R. Lloyd, and Carin K. Vanderpool. "Depletion of Glycolytic Intermediates Plays a Key Role in Glucose-Phosphate Stress in Escherichia Coli." Journal of Bacteriology 195, no. 21 (November 1, 2013): 4816–25. https://doi.org/10.1128/JB.00705-13.

Ryan, K. R., J. A. Taylor, and L. M. Bowers. "The BAM Complex Subunit BamE (SmpA) Is Required for Membrane Integrity, Stalk Growth and Normal Levels of Outer Membrane -Barrel Proteins in Caulobacter Crescentus." Microbiology 156, no. 3 (March 1, 2010): 742–56. https://doi.org/10.1099/mic.0.035055-0.

Schlimpert, Susan, Eric A. Klein, Ariane Briegel, Velocity Hughes, Jörg Kahnt, Kathrin Bolte, Uwe G. Maier, et al. "General Protein Diffusion Barriers Create Compartments within Bacterial Cells." Cell 151, no. 6 (December 7, 2012): 1270–82. https://doi.org/10.1016/j.cell.2012.10.046.

Stankeviciute, Gabriele, Ziqiang Guan, Howard Goldfine, and Eric A. Klein. "Caulobacter Crescentus Adapts to Phosphate Starvation by Synthesizing Anionic Glycoglycerolipids and a Novel Glycosphingolipid." MBio 10, no. 2 (02 2019). https://doi.org/10.1128/mBio.00107-19.

Stankeviciute, Gabriele, Amanda V. Miguel, Atanas Radkov, Seemay Chou, Kerwyn Casey Huang, and Eric A. Klein. "Differential Modes of Crosslinking Establish Spatially Distinct Regions of Peptidoglycan in Caulobacter Crescentus." Molecular Microbiology 111, no. 4 (April 2019): 995–1008. https://doi.org/10.1111/mmi.14199.

Wagner, Jennifer K., and Yves V. Brun. "Out on a Limb: How the Caulobacter Stalk Can Boost the Study of Bacterial Cell Shape: How and Why Bacteria Make Stalks." Molecular Microbiology 64, no. 1 (March 16, 2007): 28–33. https://doi.org/10.1111/j.1365-2958.2007.05633.x.

Wagner, Jennifer K., Cheryl D. Galvani, and Yves V. Brun. "Caulobacter Crescentus Requires RodA and MreB for Stalk Synthesis and Prevention of Ectopic Pole Formation." Journal of Bacteriology 187, no. 2 (January 15, 2005): 544–53. https://doi.org/10.1128/JB.187.2.544-553.2005.

Wagner, Jennifer K., Sima Setayeshgar, Laura A. Sharon, James P. Reilly, and Yves V. Brun. "A Nutrient Uptake Role for Bacterial Cell Envelope Extensions." Proceedings of the National Academy of Sciences of the United States of America 103, no. 31 (August 1, 2006): 11772–77. https://doi.org/10.1073/pnas.0602047103.

Yakhnina, Anastasiya A., and Zemer Gitai. "Diverse Functions for Six Glycosyltransferases in Caulobacter Crescentus Cell Wall Assembly." Journal of Bacteriology 195, no. 19 (October 2013): 4527–35. https://doi.org/10.1128/JB.00600-13.

Yang, Desirée C., Kris M. Blair, and Nina R. Salama. "Staying in Shape: The Impact of Cell Shape on Bacterial Survival in Diverse Environments." Microbiology and Molecular Biology Reviews: MMBR 80, no. 1 (March 2016): 187–203. https://doi.org/10.1128/MMBR.00031-15.

Young, Kevin D. "The Selective Value of Bacterial Shape." Microbiology and Molecular Biology Reviews: MMBR 70, no. 3 (September 2006): 660–703. https://doi.org/10.1128/MMBR.00001-06.

Zhu, Yingxi, and Steve Granick. "Limits of the Hydrodynamic No-Slip Boundary Condition." Physical Review Letters 88, no. 10 (February 26, 2002): 106102. https://doi.org/10.1103/PhysRevLett.88.106102.

Supplemental References:

1.Nierman WC, Feldblyum TV, Laub MT, Paulsen IT, Nelson KE, Eisen JA, et al. Complete genome sequence of Caulobacter crescentus. Proc Natl Acad Sci U S A. 2001;98(7):4136-41.

2.Evinger M, Agabian N. Envelope-associated nucleoid from Caulobacter crescentus stalked and swarmer cells. J Bacteriol. 1977;132(1):294-301.
3.Stankeviciute G, Guan Z, Goldfine H, Klein EA. Caulobacter crescentus adapts to phosphate starvation by synthesizing anionic glycoglycerolipids and a novel glycosphingolipid. MBio. 2019;10(2).

4.Simon R, Priefer U, Puhler A. A broad host range mobilization system for in vivo genetic engineering: transposon mutagenesis in gram negative bacteria. Bio/Technology. 1983;1:784.

5.Alley MR, Gomes SL, Alexander W, Shapiro L. Genetic analysis of a temporally transcribed chemotaxis gene cluster in Caulobacter crescentus. Genetics. 1991;129(2):333-41.

6.Thanbichler M, Iniesta AA, Shapiro L. A comprehensive set of plasmids for vanillate- and xylose-inducible gene expression in Caulobacter crescentus. Nucleic Acids Res. 2007;35(20):e137.

7. Jeong, Haeyoung, Hyun Ju Kim, and Sang Jun Lee. “Complete Genome Sequence of Escherichia Coli Strain BL21.” *Genome Announcements* 3, no. 2 (March 19, 2015).

8. Novo, M. Teresa Marques, Andrea Soares-Costa, Antonia Q. L. de Souza, Ana Carolina M. Figueira, Gustavo C. Molina, Carlos A. Palacios, Claudia R. Kull, Izabel F. Monteiro, Paulo H. Baldan-Pineda, and Flavio Henrique-Silva. “A Complete Approach for Recombinant Protein Expression Training: From Gene Cloning to Assessment of Protein Functionality*.” *Biochemistry and Molecular Biology Education* 33, no. 1 (2005): 34–40.